PAPER PUBLISHED IN
Marine and Petroleum Geology
Volume 69, January 2016, Pages 38–52

doi:10.1016/j.marpetgeo.2015.10.010

Origin of the Breno and Esino dolomites in the western Southern Alps (Italy): Implications for a volcanic influence

Yong Hou [a, *], Karem Azmy [a], Fabrizio Berra [b], Flavio Jadoul [b], Nigel J.F. Blamey [c], Sarah A. Gleeson [d], Uwe Brand [c]

[a] Department of Earth Sciences, Memorial University of Newfoundland, St. John's, NL, A1B 3X5, Canada

[b] Dipartimento di Scienze della Terra ñA. Desioò, Università di Milano, Via Mangiagalli 34, 20133 Milan, Italy

[c] Department of Earth Science, Brock University, St. Catharines, ON, L2S 3A1, Canada

[d] Department of Earth and Atmospheric Sciences, University of Alberta, Edmonton, Alberta T6G 2E3, Canada

Corresponding author: Yong Hou, E-mail address: yh3858@mun.ca

Abstract

The Esino Limestone of the western Southern Alps represents a differentiated Ladinian-Lower Carnian (?) carbonate platform comprised of margin, slope and peritidal inner platform facies up

to 1000m thick. A major regional subaerial exposure event lead to coverage by another peritidal Lower Carnian carbonate platform (Breno Formation). Multiphase dolomitization affected the carbonate sediments. Petrographic examinations identified at least three main generations of dolomites (D1, D2, and D3) that occur as both replacement and fracture-ýlling cements. These phases have crystal-size ranges of 3 to 35ε m (dolomicrite D1), 40 to 600ε m (eu- to subhedral crystals D2), and 200ε m to 5mm (cavity- and fracture-filling anhedral to subhedral saddle dolomite D3), respectively.

The fabric retentive near-micritic grain size coupled with low mean Sr concentration (76 ± 37 ppm) and estimated ŭ^{18}O of the parent dolomitizing fluids of D1 suggest formation in shallow burial setting at temperature ~ 45 - 50 ºC with possible contributions from volcanic-related fluids (basinal fluids circulated in volcaniclastics or related to volcanic activity), which is consistent with its abnormally high Fe (4438 ± 4393 ppm) and Mn (1219 ± 1418 ppm) contents. The larger crystal sizes, homogenization temperatures (D2, 108 ± 9 ºC; D3, 111 ± 14 ºC) of primary two-phase þuid inclusions, and calculated salinity estimates (D2, 23 ± 2 eq wt% NaCl; D3, 20 ± 4 eq wt% NaCl) of D2 and D3 suggest that they formed at later stages under mid- to deeper burial settings at higher temperatures from dolomitizing fluids of higher salinity, which is supported by higher estimated ŭ^{18}O values of their parent dolomitizing fluids. This is also consistent with their high Fe (4462 ± 4888 ppm; and 1091 ± 1183 ppm, respectively) and Mn (556 ± 289 ppm and 1091 ± 1183 ppm) contents, and low Sr concentrations (53 ± 31 ppm and 57 ± 24 ppm, respectively).

The similarity in shale-normalized (SN) REE patterns and Ce $(Ce/Ce^*)_{SN}$ and La $(Pr/Pr^*)_{SN}$ anomalies of the investigated carbonates support the genetic relationship between the dolomite

generations and their calcite precursor. Positive Eu anomalies, coupled with fluid-inclusion gas ratios (N_2/Ar, CO_2/CH_4, Ar/He), high F^- concentration, high F/Cl and high Cl/Br molar ratios suggest an origin from diagenetic fluids circulated through volcanic rocks, which is consistent with the co-occurrence of volcaniclastic lenses in the investigated sequence.

Keywords: Carbonate diagenesis; Dolomitization; stable isotopes; Rare Earth Elements; Microthermometry; Fluid-inclusion gases; Triassic; western Southern Alps (Italy).

1. Introduction

This study has been focused on the dolomites that might have formed from diagenetic fluids derived from magma or from the interaction between volcaniclastic deposits and water circulating thorough them. To investigate the possible causal relationship between volcanic activity and dolomitization, it is important to identify successions where the dolomites occur in carbonate facies having volcanic or volcaniclastic deposits. The presence of these deposits may affect the composition of the fluids responsible for dolomitization and the geochemical fingerprints are expected to be recorded in the dolomites. A favorable scenario for this type of dolomites is presented by the Triassic succession of the Southern Alps of Italy (Fig. 1), where dolomitized platform facies are associated with volcaniclastic deposits (Fig. 2).

In the Southern Alps, crustal movements and volcanic activity took place during Middle and Late Triassic (Castellarin et al. 1979; Pisa et al., 1979, Brusca et al., 1981), and volcanogenic sediments (volcaniclastic sandstones, volcanic conglomerate and tuffs) have been extensively preserved within Anisian - Carnian carbonate sequences (Jadoul and Rossi, 1982; Crisci et al., 1984; Obenholzner, 1991). The carbonate units of the western Southern Alps (Esino Limestone,

Calcare Rosso, Breno Formation and Calcare Metallifero Bergamasco) coeval with the volcaniclastic inputs are locally dolomitized and host important Pb-Zn mineralization (Assereto et al., 1979; Brusca et al., 1981). Therefore, the study of petrography and geochemistry of these dolomites is ideal to understand the possible role of volcanic activity in the development of the associated dolomites. The current investigation is a multi-approach study focused on the evaluation of possible contribution of volcanic activity to dolomitization of carbonates via petrographic and geochemical examination including microthermometry, fluid-inclusion gas ratios, stable isotopes, major and minor and rare earth elements (REE), and halogens.

The main objectives of this study are to:

1. Investigate the petrographic and geochemical characteristics and diagenetic evolution of the Esino and Breno dolomites, which are associated with volcaniclastic sandstones and volcanic deposits (mostly tuffs), in the western Southern Alps of Italy.

2. Identify and characterize (petrographically and geochemically) the dolomitization phases and investigate the characteristics and nature of their parent dolomitizing fluids.

3. Investigate the influence of volcaniclastic deposits (or volcanic activity if associated) on the chemical signatures of the associated dolomites.

2. Geological setting

The study area belongs to the western part of the Southern Alps, bordered by the Insubric Line in the north and by the Po plain in the south. In detail, the studied outcrops are placed in the western part (Lombardy) of the Southern Alps (Fig. 1; e.g., Feist-Burkhardt et al., 2008). The

region underwent several subsidence events and sea-level fall cycles during the Triassic (Jadoul and Rossi, 1982; Gaetani et al., 1998; Berra and Carminati, 2010) and intense deformation during the Alpine orogenesis. During the Ladinian and Carnian, this part of the Tethyan domain recorded major paleogeographic changes, with the stratigraphic evolution from a high relief platform system with intraplatform deep troughs (Ladinian) to mixed deposits consisting of volcaniclastic fluvio-deltaic systems bordered by lagoon in front of a peridiдal carbonate platform (Early Carnian, Assereto and Casati, 1965).

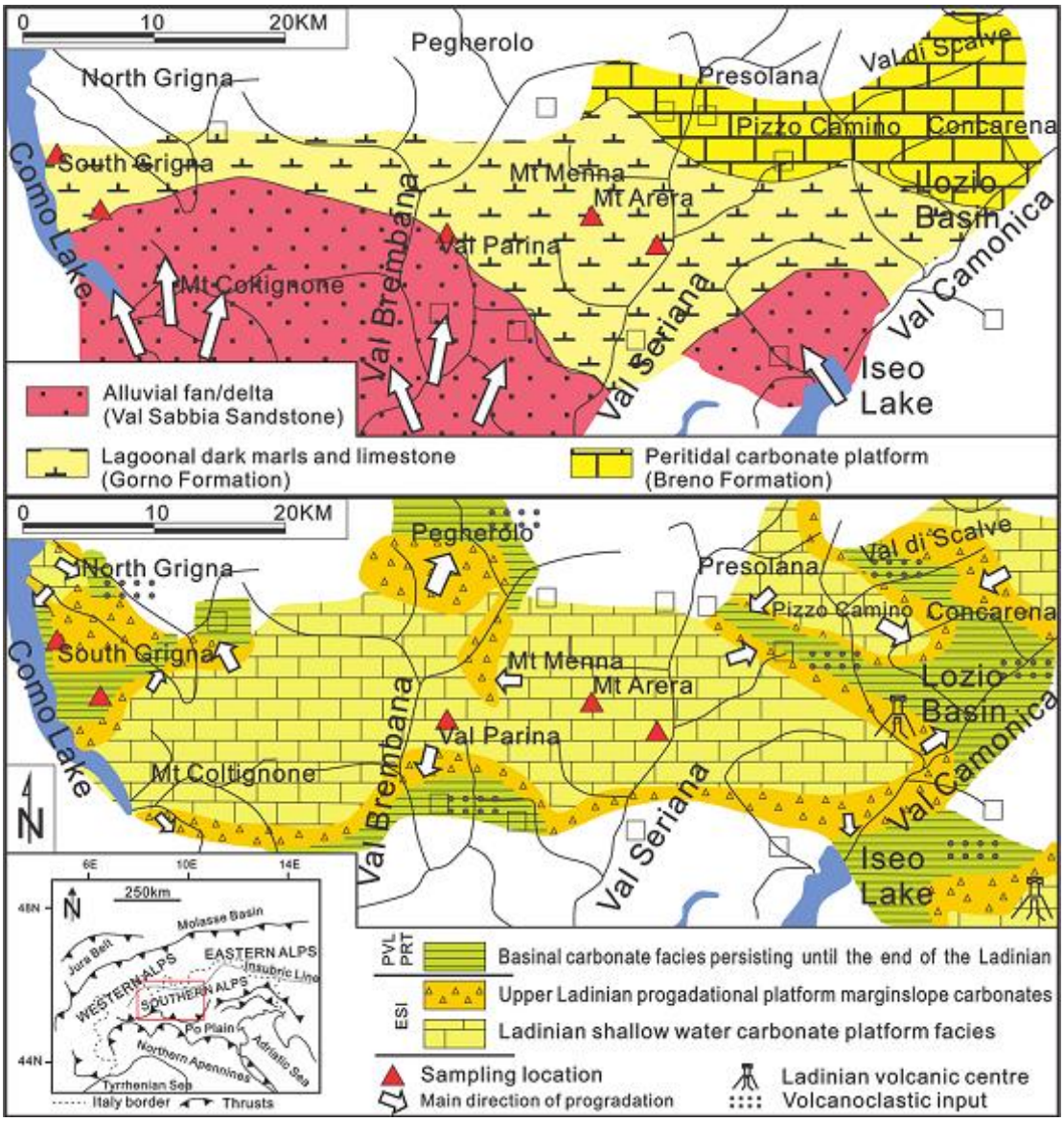

Fig. 1. Late Ladinian (below, modified after Berra et al., 2011) and early Carnian (above, modified after Brusca et al., 1981) palaeogeography of the western Southern Alps with inset of simpliýed tectonic map of Northern Italy (modiýed from Ronchi et al., 2011).

The studied dolomites come from two different carbonate platforms (Fig. 2) that belong to different evolutionary stages in the western Southern Alps: a high relief, isolated Ladinian system and a Lower Carnian inner platform. The Ladinian sediments are characterized by thick

carbonate platforms with steep-slopes (Esino Limestone) and a rapid progradation in its upper part. Inner platform facies in the core of the platform are separated by a narrow reef belt from slope breccias (Jadoul et al., 1992; Berra et al., 2012). This unit (up to 1000m) is bordered by basinal successions consisting of re-sedimented limestones and volcaniclastic sandstones (e.g., Assereto and Casati, 1965; Jadoul et al., 1992, Berra and Carminati, 2012). In the Southern Alps, at the end of the Ladinian, most of the intraplatform seaways were closed due to the intense progradation of the platform (Berra et al., 2011) so that sedimentation was dominated by shallow-water carbonates (Jadoul et al., 1992; Berra, 2007).

Close to the Ladinian-Carnian boundary, a major sea-level fall was responsible for the subaerial exposure of the top of the Esino Limestone platform, followed by a general reorganization of the facies distribution. The repeated subaerial exposure of the platform top accounts for the development of palaeokarsts and tepee horizons at the top of Esino Formation (Assereto et al., 1977), which is also indicated by the occurrence of a thin wedge of peritidal limestone, residual breccias and terra-rossa deposits (Calcare Rosso Formation, Assereto and Kendall, 1971, 1977; Mutti, 1994; Jadoul et al., 2002: Berra, 2012, Vola and Jadoul 2014) overlying the Esino Limestone. Tuff and volcanic deposits are also locally present at the top of the Esino Limestone and in the Breno Formation, indicating coeval volcanic activity in the surrounding areas close to the Ladinian-Carnian boundary.

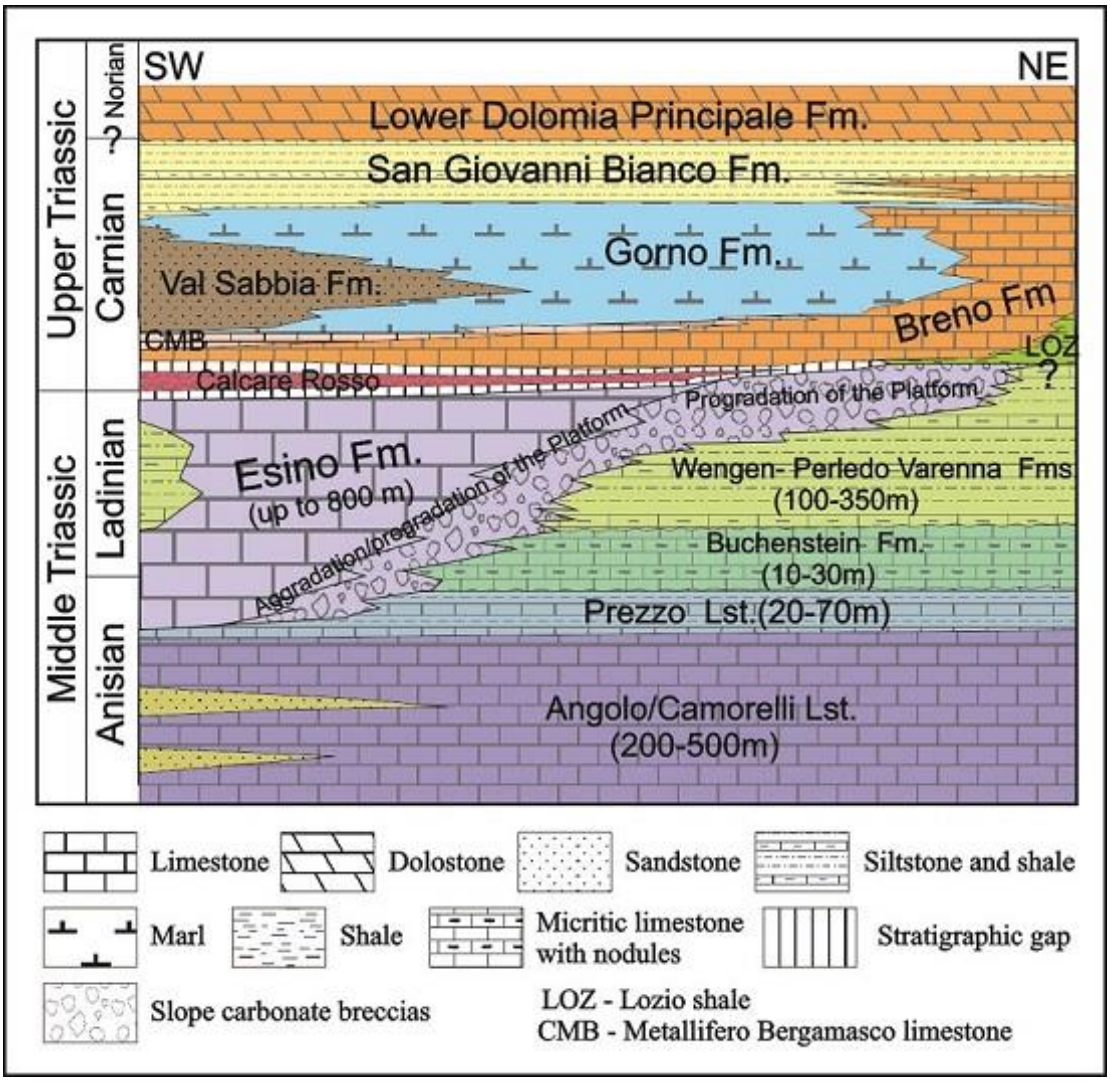

Fig. 2. Facies and stratigraphic framework of Middle-Upper Triassic sediments of the western Southern Alps (modified from Assereto and Folk, 1980).

After the subaerial exposure, the depositional system records a major event of paleogeographic reorganization (Assereto and Casati, 1965). In the northern sector, peritidal carbonate platform facies (Breno Formation) covered by lagoonal dark limestone (Calcare Metallifero Bergamasco) were deposited (Gnaccolini and Jadoul 1990; Berra and Jadoul, 2002), recording the drowning of the carbonate platform. Alluvial fan and deltaic volcaniclastic sandstones, prograding northward,

prevail toward the south (Val Sabbia Sandstone, Gnaccolini, 1983; Garzanti, 1985). Between these sandstones and the northern carbonate platform (Breno Formation), lagoonal facies were deposited (Gorno Formation; Gnaccolini, 1986; Gnaccolini, 1988; Gnaccolini and Jadoul, 1988). The petrographic composition of the prograding deltaic bodies reveals the erosion of volcanic edifices (Garzanti, 1985) originally developed in the area presently occupied by the Po Plain. The overlying San Giovanni Bianco Formation (SGB) records the end of this paleogeographically complex scenario, with the development of coastal to sabkha facies (Garzanti et al., 1995) that can be traced, with different lithostratographic names, all across for most of the Southern Alps of Italy (San Giovanni Bianco Formation in the western Southern Alps; Travenanzes Formation, upper Raibl Group in the central and eastern Southern Alps).

During the Ladinian, intense volcanic activity is well-documented in the Southern Alps, where thick lava flows are coeval with the Ladinian carbonate platforms (e.g., Bosellini and Rossi, 1974a, 1974b; Castellarin et al; 1979; Brusca et al., 1981; Bosellini et al., 2003; Berra et al., 2011). In the western Southern Alps, the evidence of volcanism is provided mostly by deep-water volcaniclastic deposits (Wengen Formation) preserved in the deep intraplatform troughs (Assereto and Casati, 1965). An early Carnian volcanic activity is further recorded in the sediments of the western Southern Alps (Brusca et al., 1981), but its significance is unclear. This volcanism is identified by tuffs and minor proximal volcanic deposits, which are discontinuously preserved in the peritidal facies of the Breno Formation (Assereto et al., 1977).

3. Methodology

3.1. Sampling

Samples were collected from limestones and dolomites at abandoned mines (Resinelli, Pedrozio, Arera and Trevasco) from Esino and Breno formations in the western Southern Alps of Lombardy (Figs. 1 and 2; Appendix 1). The distribution of the sampling sites defines an east-west oriented belt that follows the outcrops of the Ladinian-Carnian boundary and the top of lower Carnian (Breno Formation) peritidal carbonates. Samples are mostly derived from the peritidal facies of the Breno Formation, the unit that hosts the most important Pb-Zn ore bodies and for the miners represents a morphologic and stratigraphic marker (from a few tens to 150 m thick), called ñ*Metallifero*ò. This unit is bracketed between a unit recording multiple episodes of subaerial exposure at the base (Calcare Rosso) and the drowning recorded by subtidal lagoonal facies of the Calcare Metallifero Bergamasco, in turn covered by the lagoonal facies of the Gorno Formation or by the volcaniclastic deposits of the Val Sabbia Sandstone.

3.2. Petrography

Petrographic analyses were carried out by the examination of thin sections under a standard polarizing microscope and cathodoluminoscope (CL). The thin sections were cut at standard thickness (30 μm), polished, and stained with a mixture solution of Alizarin Red-S and potassium ferricyanide (Dickson, 1966). Cathodoluminescence was performed using a Technosyn cold cathodoluminoscope operated at 12kV accelerating voltage and 0.7mA gun current intensity whereas the UV luminescence was by a CRAIC-QDI 202 UV luminescope mounted on a Zeiss imager D1m microscope. A mirror-image slab of each thin section was also

polished and cleaned with deionized water for micro-sampling of different carbonate generations for geochemical analyses.

3.3. Microthermometry

Fluid-inclusion microthermometric (Appendix 2) measurements were performed on double polished wafers (about 80μm thick) using a Linkam THMSG600 heating-freezing stage at Memorial University of Newfoundland (MUN). Precision of ±0.1 °C at -56.6 °C and ±0.3 °C at 374.1 °C was calculated via calibration using synthetic H_2O and CO_2 fluid inclusion standards. The homogenization temperatures (T_h), initial melting temperatures (T_i), and last ice melting ($T_{m\,(ice)}$) of primary two phases fluid of dolomite and calcite generations were measured according to the procedures of Shepherd et al. (1985). Heating was carried out before freezing to avoid stretching of the inclusions due to freezing (Lawler and Crawford, 1983). The salinity estimates were calculated by applying the measured $T_{m\,(ice)}$ values to the equation of Bodnar (1993), and reported as equivalent weight percent NaCl (eq. wt% NaCl).

3.4. Geochemical analyses

Representative samples from different carbonate generations were microdrilled under a binocular microscope from the polished mirror-image slabs with a low-speed microdrill. The microdrilled spots were selected carefully to avoid cross-contamination. The slabs were previously cleaned with deionized water and dried at temperature between 30 °C and 34 °C prior to microsampling.

3.4.1. Major and minor elements

Approximately 10 mgs of sample powder was digested in 2.5% (v/v) pure HNO_3 (Coleman et al., 1989) and analyzed for Ca, Mg, Sr, Mn and Fe as well as Rare Earth Elements (REE) using a

Perkin Elmer Sciex ñElan DRCIIò ICP-MS at MUN. The REE concentrations were normalized relative to the Post-Archean Australian Shale (McLennan, 1989). Anomalies of Europium $(Eu/Eu^*)_{SN} = Eu_{SN}/ (0.67Sm_{SN} + 0.33Tb_{SN})$, Cerium $(Ce/Ce^*)_{SN} = Ce_{SN}/(0.5La_{SN} + 0.5Pr_{SN})$, and Lanthanum $(Pr/Pr^*)_{SN} = Pr_{SN}/(0.5Ce_{SN} + 0.5Nd_{SN})$ were calculated according to the formulae of Bau and Dulski (1996). The relative uncertainties are less than 5%, and results are normalized to a 100% carbonate basis (e.g. Azmy et al., 2014).

3.4.2. Stable isotopes

A subset of sample powder, each ~ 0.2 mg, was reacted in an inert atmosphere (He) with ultra-pure concentrated orthophosphoric acid at 50 ºC. The produced CO_2 was automatically þushed through a chromatographic column to the source of a Thermo Finnigan DELTA V plus isotope ratio mass spectrometer in a helium stream to be ionized and measured for isotope ratios. Uncertainties of better than 0.1ă (2σ) for the analyses were determined by repeated measurements of NBS-19 ($\delta^{18}O$ = -2.20ă and $\delta^{13}C$ = +1.95ă vs. VPDB) and L-SVECS ($\delta^{18}O$ = -26.64ă and $\delta^{13}C$ = -46.48ă vs. VPDB) as well as internal standards during each run of samples.

3.5. Fluid-inclusion gas analysis

Fluid-inclusion gas analysis was performed by the crush-fast scan (CFS) method (Norman and Moore, 1997; Norman and Blamey, 2001; Parry and Blamey, 2010; Blamey, 2012; Azmy and Blamey, 2013; Blamey et al., 2015) at the New Mexico Institute of Mining and Technology (NMT) Fluid Inclusion Gas laboratory. Samples were gently crushed by hand and sieved in 30-mesh sieve, where the smaller fraction was discarded. The 30-mesh size fraction was cleaned

with 20% KOH, rinsed several times with deionized water, and dried below 100°C. Approximately 200mg of each sample was incrementally crushed under a vacuum of approximate 10^{-8} Torr, producing up to 10 crushes analyzed by two Pfeiffer-Vacuum Prisma quadrupole mass spectrometers. The measured volatiles include H_2, He, CH_4, H_2O, N_2, O_2, H_2S, Ar, and CO_2. The system calibration was performed using commercial gas mixtures and three in-house þuid inclusion gas standards following the technique described by Norman and Blamey (2001) and Blamey et al. (2015). H_2 is reliably detected at 50 ppm, He at <0.5 ppm. Precision for the major gas species CO_2, CH_4, N_2, and Ar is better than 5 %, whereas it is ~10 % for the minor species.

3.6. Halogens analysis

The halogens analyses were performed by the bulk fluid crush-leach method (Banks and Yardley, 1992; Gleeson and Turner, 2007; Bernal et al., 2014) at the Department of Earth and Atmospheric Sciences, University of Alberta. The samples were crushed and sieved to obtain ~ 2g with a grain size of 1-2mm. Each mineral separate was washed, dried, ground to ýne powder, and mixed in a vial with 5ml of de-ionized water. The samples were shaken, and ýltered through 0.45µm PTFE ýlters. The leachate was run in on a Dionex DX600 ion chromatograph (IC) with an AS14A anion column (Cl, Br, F, and sulfate). A seven anion standard solution, pure water blanks and an internal quality control standard were run after every 10 unknowns. The data were reproducible to 5%. The detection limits were 0.03mg/L for Cl^-, Br^-, and 0.01mg/L for F^-.

4. Results

4.1. Petrography

The Esino and Breno formations in western Southern Alps consist of limestone and dolostone lithofacies. The limestone lithofacies include mudstone, wackstone, packstone, and fine to coarse crystalline carbonate (e.g., Gnaccolini and Jadoul, 1990; Bertotti et al., 1993; Jadoul and Weissert, 1989; Berra et al. 2011; Berra and Carminati; 2012). The dolostone lithofacies vary from fine grained (3ε m) dolomicrites to coarse grained (5mm) saddle dolomites. The dolomite generations occur as both replacement and cements (Fig. 3).

Petrographic examination indicates multiple generations of crystallization for both calcite and dolomite. The calcite generations (Fig. 3), from the earliest to the latest, are micrite (microbial mud) and fibrous cement (C1, Fig. 3a, b), pore-ýlling equant calcite (C2, 25 - 400μm, Fig. 3b), and coarse fracture filling calcite (C3, 200μm - 15mm, Fig. 3e, g). Under cold cathodoluminoscope, C1 and C2 exhibit dull to non-CL (Fig. 3b) but calcite C3 exhibits bright orange CL (Fig. 3f, h). The dolomite generations (Fig. 3), also from the earliest to the latest, are dolomicrite (D1, Fig. 3d, e), equant replacive dolomite (D2, Fig. 3d, g), and large fracture-ýlling saddle dolomite (D3, Fig. 3e, i). Calcite C3 and dolomite D3 fill the fractures that crosscut earlier calcite and dolomite generations. The paragenetic sequence of events, based on petrographic relationships observed in the Esino and Breno carbonates, is summarized in Figure 4.

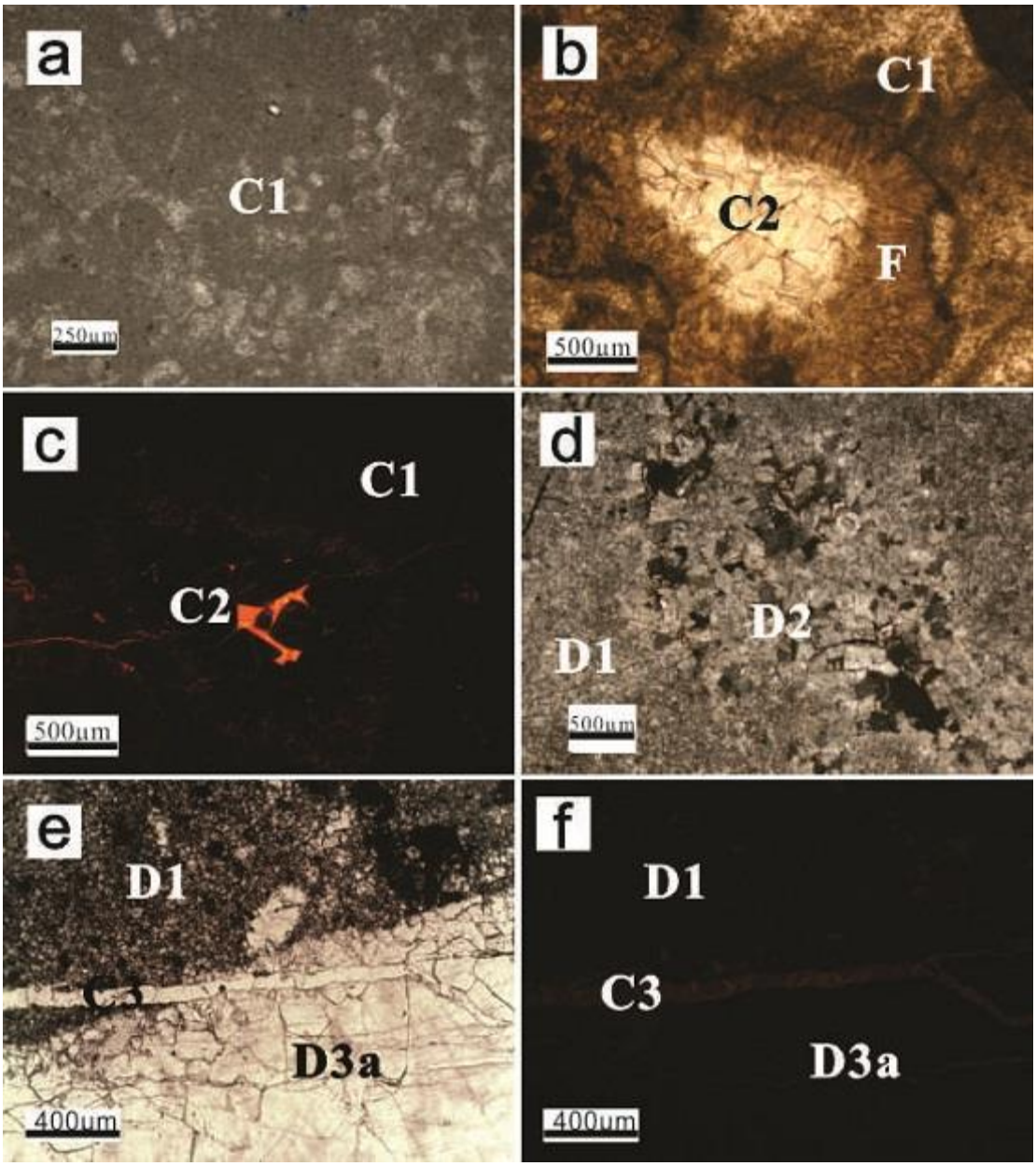
a
C1
250μm
b
C1
C2
F
500μm
c
C1
C2
500μm
d
D2
D1
500μm
e
D1
C3
D3a
400μm
f
D1
C3
D3a
400μm

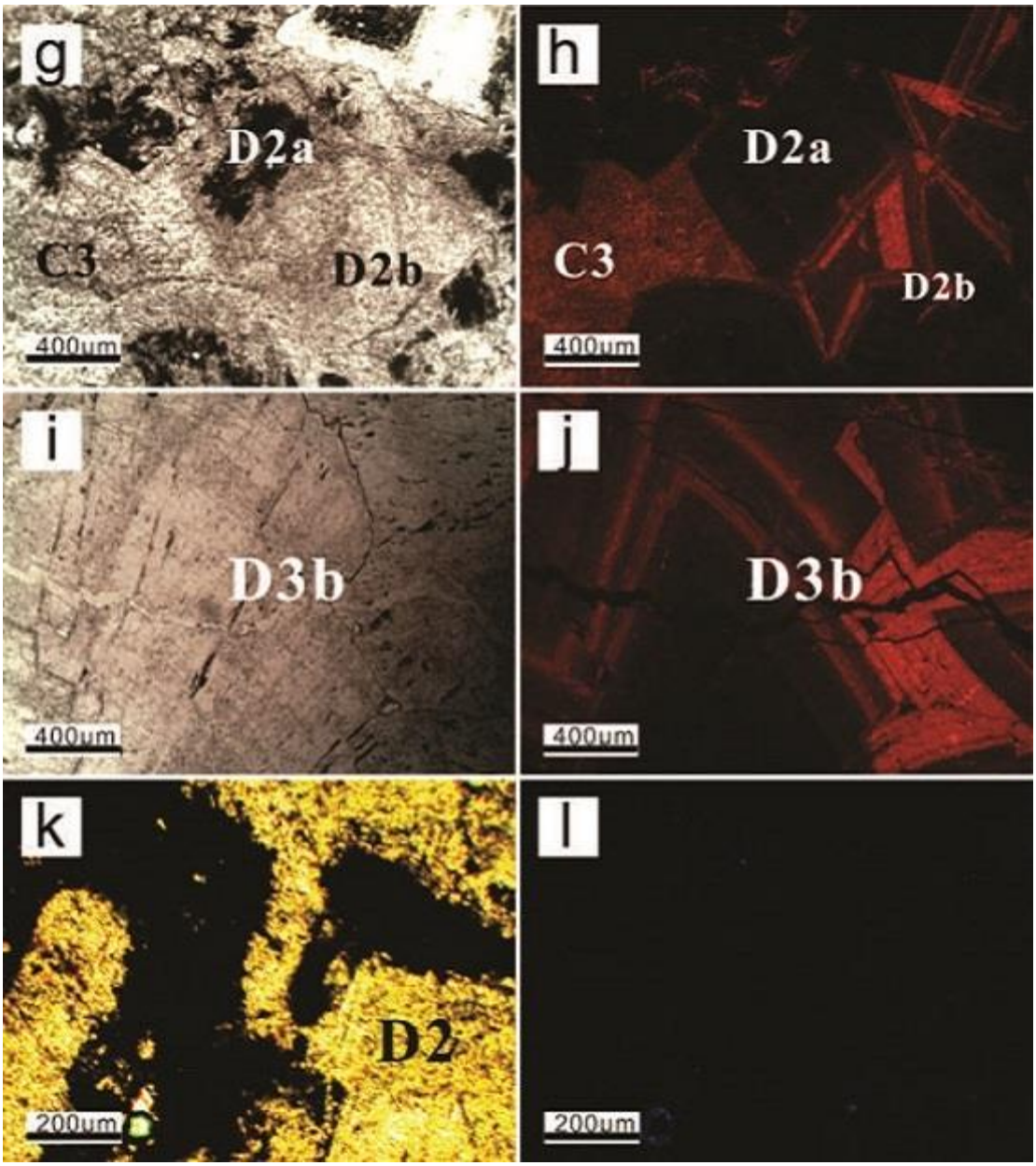

Fig. 3. Photomicrographs of petrographic features of Esino and Breno carbonates. (a) Calcite C1 (plane polarized; Sample PE1), (b) Calcite C2 and fibrous cement F (crossed polars; Sample PE7), (c) Cathodoluminescence image of (b) showing dull CL of C1 and C2, (d) Dolomite D1 and D2 (crossed polars; Sample ES), (e) Dolomite D1, D3a and calcite C3 (plane polarized; Sample PE8), (f) Cathodoluminescence image of (e) showing dull CL in D1 and D3a, (g) Dolomite D2a, D2b and calcite C3 showing organic matter along zones in D2a crystals (plane

polarized; Sample BR), (h) Cathodoluminescence image of (g) showing dull CL of D2a, zonation CL of D2 and bright orange CL of C3, (i) Saddle dolomite D3b with undulose extinction (crossed polars; Sample BR3), (j) Cathodoluminescence image of (i) showing zonation CL of D3b, (k) D2 with organic material around the crystal rim (crossed polars; Sample BR), and (l) Ultraviolet image of (k) showing no þorescence of the organic matter.

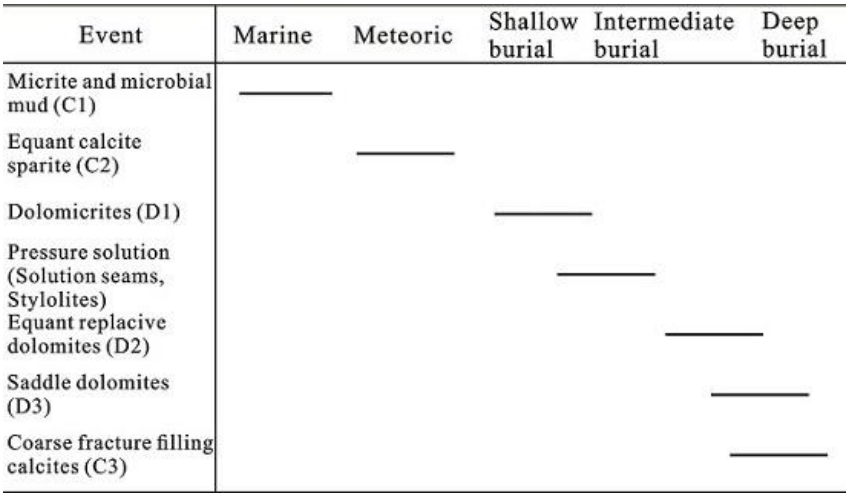

Fig. 4. Paragenetic sequence of the main diagenetic events that influenced the Esino and Breno carbonates based on petrographic relationships.

The early dolomite (D1) consists of replacive, fabric retentive, near-micritic to non-planar mosaic crystals (Fig. 3d, e) ranging from 3 to 35εm with irregular intercrystalline boundaries. D1 is nonporous under standard polarizing microscope with dull to non-CL image (Fig. 3f) and is crosscut occasionally by microstylolites. D2 is a replacive fabric destructive dolomite and consists of eu- to subhedral crystals ranging from 30 to 600εm where crystals may have cloudy cores with clear rims (Fig. 3d, g). D2 exhibit dull (D2a, Fig. 3h) to, at times, concentric zoning under CL (D2b, Fig. 3h). Like D1, D2 is crosscut by the late fractures, which are filled with the

latest D3 and C3. Organic material is visible around the crystal rims of D2 and also marks their growth zones inside the crystals but shows no þuorescence under UV (Fig. 3k, l). The D3 is fracture-ýlling, coarse (250µm - 5mm) an- to subhedral crystals of saddle dolomite with typical undulose extinction (Fig. 3e, i) and dull CL (D3a, Fig. 3f) to less common concentric zoning (D3b, Fig. 3j) like D2. All the dolomite and calcite generations are nonporous.

4.2. Fluid inclusions

The primary two-phase (liquid + vapour) fluid inclusion (Goldstein and Reynolds, 1994) were measured in D2 and D3, as well as C3, which have larger crystals (Appendix 2) but no measurements were obtained from D1 (dolomicrite) because of the small crystal sizes. The measured inclusions have relatively consistent liquid: vapour ratios (~ 0.95) and narrow range (less than 15 ºC) of homogenization temperatures (Goldstein and Reynolds, 1994, Bodnar, 2003). The homogenization temperatures (T_h), initial melting temperatures (T_i), ýnal melting temperatures of ice ($T_{m\,(ice)}$), and calculated salinities as well as their statistics are presented in Appendix 2 and summarized in Table 1 and Figure 5a-d.

Table 1. Statistics of microthermometric measurements of the investigated carbonates.

Host mineral	Size		T_i (°C)	$T_{m\,(ice)}$ (°C)	Eq. wt% NaCl	T_h (°C)
D2	2 - 20µm	*n*	1	44	44	58
		Mean	-43	-21	23	108
		S.D.		3	1.7	9
		Max	-43	-15	27	128
		Min	-43	-27	19	94
D3	2 - 30µm	*n*	77	104	104	108
		Mean	-32	-18	20	111
		S.D.	8	6	4	14
		Max	-18	-8	30	144
		Min	-51	-32	12	86

C3	3 - 50μm	*n*	66	63	63	80
		Mean	-41	-20	22	112
		S.D.	7	6	5	9
		Max	-21	-8	29	140
		Min	-52	-31	12	91

The mean values of T_h, (Table 1; 108 ± 9 ºC， n = 58, 111 ± 14 ºC， n = 108, and 112 ± 9 ºC， n = 80, respectively), $T_{m\,(ice)}$ (Table 1; -21 ± 3 ºC, n = 44, -18 ± 6 ºC, n = 104, and -20 ± 6 ºC, n = 63) and salinity estimates (Table 1; 23 ± 2 eq wt% NaCl, n = 44, 20 ± 4 eq wt% NaCl, n = 104, and 22 ± 5 eq wt% NaCl, n = 63, respectively) of D2, D3 and C3 did not vary dramatically.

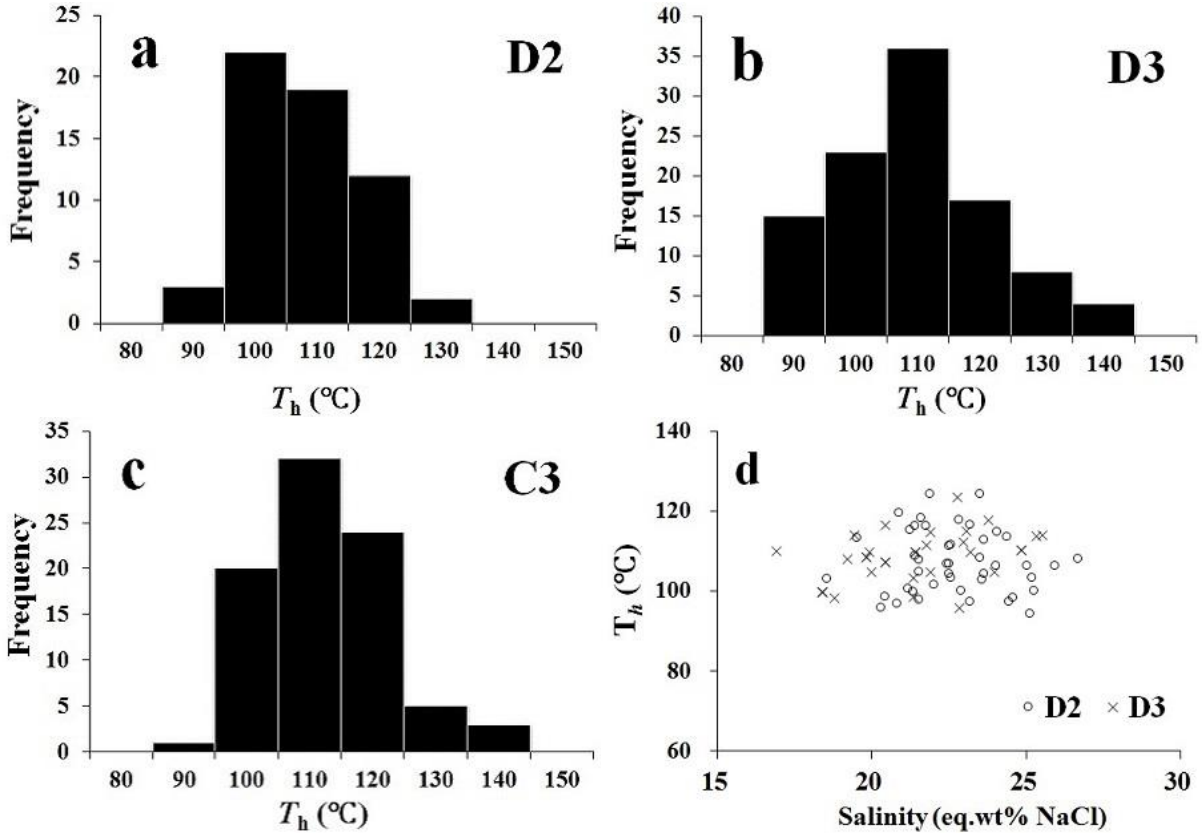

Fig. 5. Plots of the microthermometric data of primary two-phase þuid inclusions trapped in D2, D3 and C3, showing histograms of homogenization temperature of (a) D2, (b) D3, and (c) C3,

and a scatter diagram (d) of estimated salinity (Bodnar, 2003) vs. homogenization temperatures of D2 and D3.

4.3. Carbon and oxygen isotopes

Table 2 summarizes the carbon and oxygen isotopic compositions of the investigated carbonates (Appendix 1). The mean ŭ^{13}C and ŭ^{18}O values of C3 are more depleted than those of C1 (+0.7 ± 0.6ă VPDB, *n* = 9 and -9.3 ± 2.7ă VPDB, *n* = 9 vs. +1.0 ± 0.9ă VPDB, *n* = 18 and -7.9 ± 1.8ă VPDB, *n* = 18, respectively). The mean ŭ^{13}C values increase slightly from D1 (1.7 ± 0.6ă VPDB, *n* = 20) to D2 (1.8 ± 0.3ă VPDB, *n* = 8) and the latest D3 (1.9 ± 0.5ă VPDB, *n* = 25), but the mean ŭ^{18}O values decrease through time although the change is also insignificant between D2 and D3 (D1 = -5.9 ± 3.3ă VPDB, *n* = 20; D2 = -8.4 ± 1.2ă VPDB, *n* = 8; and D3 = -9.0 ± 1.0ă VPDB, *n* = 25, respectively). C3 has the lowest mean ŭ^{13}C and ŭ^{18}O values among all the investigated calcites and dolomites (Table 2).

Table 2. $CaCO_3$, $MgCO_3$, Mn, Sr, Fe, ŭ^{18}O and ŭ^{13}C statistics of the investigated Esino and Breno carbonates in the western Southern Alps.

Phase		$CaCO_3$%	$MgCO_3$%	Fe (ppm)	Mn (ppm)	Sr (ppm)	ŭ^{13}Că (VPDB)	ŭ^{18}Oă (VPDB)
C1	*n*	36	36	36	36	36	18	18
	Mean	98.2	1.8	217	203	237	1.0	-7.9
	S.D.	1.5	1.5	153	131	123	0.9	1.8
	Max	99.4	7.1	703	565	606	1.8	-5.2
	Min	92.9	0.6	56	56	146	-1.1	-13.2
C3	*n*	18	18	18	18	18	9	9
	Mean	97.6	2.4	805	1328	178	0.7	-9.3
	S.D.	1.8	1.8	1111	1192	192	0.6	2.7
	Max	99.4	5.6	3788	3655	649	1.6	-5.2
	Min	94.4	0.6	74	102	47	0.0	-13.0
D1	*n*	33	33	40	40	40	20	20

	Mean	56.4	43.6	4438	1219	76	1.7	-5.9
	S.D.	3.9	3.9	4393	1418	37	0.6	3.3
	Max	64.6	51.3	16735	4863	155	2.6	-0.8
	Min	48.7	35.4	289	122	27	0.7	-10.2
D2	*n*	17	17	22	22	22	8	8
	Mean	54.6	45.4	1460	556	53	1.8	-8.4
	S.D.	6.0	6.0	900	289	31	0.3	1.2
	Max	62.9	55.3	3162	1078	125	2.3	-6.6
	Min	44.7	37.1	276	156	18	1.3	-9.8
D3	*n*	49	49	53	53	53	25	25
	Mean	55.3	44.7	4462	1091	57	1.9	-9.0
	S.D.	5.4	5.4	4888	1183	24	0.5	1.0
	Max	64.9	54.9	24955	6049	151	2.9	-6.1
	Min	45.1	35.1	714	266	31	0.9	-10.4

4.4. Major and minor elements

The results of major and minor elements of Esino and Breno carbonates are presented in Appendix 1 and summarized in Table 2. They indicate that the investigated dolomites are near stoichiometric and have around the same Mg concentrations ($MgCO_3$%, D1, 43.6 ± 3.9%, *n* = 33; D2, 45.4 ± 6.0%, *n* = 17; D3, 44.7 ± 5.4%, *n* = 49).

D2 has the lowest mean Fe (1460 ± 900, *n* = 22) and Mn (556 ± 289 ppm, *n* = 22) concentrations relative to those of D1 (Fe = 4438 ± 4393 ppm, *n* = 40 and Mn = 1219 ± 1418 ppm, *n* = 40, respectively) and D3 (Fe = 4462 ± 4888 ppm, *n* = 53 and Mn = 1091 ± 1183 ppm, *n* = 53, respectively). D2 and D3 have similar Sr concentrations (53 ± 31 ppm, *n* = 22 and 57 ± 24 ppm, *n* = 53, respectively), which are lower than those of D1 (76 ± 37 ppm, *n* = 40). Calcites have lower mean Fe concentrations (C1 = 217± 153 ppm, *n* = 36 and C3 = 805 ± 111 ppm, *n* = 18) but higher Sr contents (C1 = 237 ± 123 ppm, *n* = 36 = C3, 178 ± 193 ppm, *n* = 18) than their dolomite counterparts (Table 2). Among all the calcite and dolomite generations, calcite C1 has

the lowest mean Fe and Mn concentrations (217 ± 153 ppm, *n* = 36 and 203 ± 131 ppm, *n* = 36, respectively) and highest Sr contents (237 ± 123 ppm, *n* = 36), whereas calcite C3 has the highest mean Mn concentrations (1328 ± 1192 ppm, *n* = 18). C2 was impossible to microsample because it is rare and always mixed with C1.

4.5. Rare earth elements (REE)

The results of the rare earth elements (REE) analyses of Esino and Breno carbonates are presented in Appendix 1 and summarized in Table 3, and Figure 6 shows the corresponding shale normalized (SN) proýles. Calcite C3 has the highest mean ×REE value (17 ± 12 ppm, *n* = 9) among all the investigated calcites and dolomites, and D1 has the highest mean value (×REE = 10 ± 9 ppm, *n* = 19) among all the dolomites but D2 has the lowest (×REE = 3 ± 1 ppm, *n* = 11).

Table 3. Summary of rare earth element concentrations in the Esino and Breno carbonates in the western Southern Alps.

Phase		La (ppb)	Ce (ppb)	Pr (ppb)	Nd (ppb)	Sm (ppb)	Eu (ppb)	Gd (ppb)	Tb (ppb)	Dy (ppb)	Ho (ppb)	Er (ppb)	Tm (ppb)	Yb (ppb)	Lu (ppb)	ΣREE (ppm)
D1	*n*	19	19	19	19	19	19	19	19	19	19	19	19	19	19	19
	Mean	1956	4146	523	2107	402	91	398	57	294	56	157	20	127	17	10
	S.D.	1830	3710	443	1758	322	76	296	39	172	31	84	10	65	9	9
	Max	7937	16176	1770	6765	1217	295	1182	148	613	113	311	38	250	35	37
	Min	316	478	74	308	57	11	64	10	52	12	34	4	35	5	2
D2	*n*	11	11	11	11	11	11	11	11	11	11	11	11	11	11	11
	Mean	702	1105	138	528	107	22	135	23	137	30	88	12	69	10	3
	S.D.	267	490	47	171	39	7	48	9	55	12	33	5	31	5	1
	Max	1298	2297	231	815	174	37	219	40	234	53	146	19	115	17	6
	Min	353	481	74	290	52	14	69	10	59	13	34	3	18	2	2
D3	*n*	26	26	26	26	26	25	26	26	26	26	26	26	26	25	26
	Mean	1564	2994	359	1350	240	56	258	34	164	30	81	9	53	7	7
	S.D.	1868	4109	495	1876	325	70	342	45	211	36	95	11	65	8	9
	Max	6943	18095	2267	8658	1569	298	1610	221	1060	182	486	55	337	40	42
	Min	186	284	37	138	27	6	27	2	25	4	11	0	11	1	1
C1	*n*	18	18	18	18	18	18	18	18	18	17	18	18	18	15	18
	Mean	1064	2013	249	968	174	39	171	23	119	24	72	10	64	11	5
	S.D.	1335	2772	357	1407	250	57	233	32	183	41	122	18	113	20	7
	Max	5640	11964	1518	5910	1000	193	838	119	757	172	531	79	494	79	28

	Min	185	313	34	124	15	4	31	0	15	2	9	0	8	0	1
C3	*n*	9	9	9	9	9	9	9	9	9	9	9	9	9	9	9
	Mean	3159	6672	802	3095	603	163	633	99	516	106	316	46	311	48	17
	S.D.	1943	4924	489	1954	473	144	523	93	527	119	359	53	377	62	12
	Max	7370	18336	1663	6607	1524	484	1546	263	1494	344	1086	157	1127	186	41
	Min	1238	2793	311	1173	219	42	242	26	86	10	34	7	21	2	7

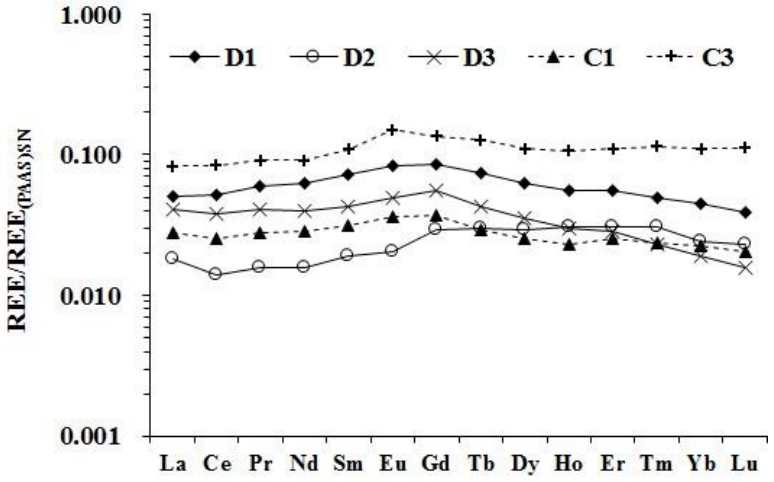

Fig. 6. Pattern of mean shale-normalized REE concentrations of the investigated calcite and dolomite generations.

There is a narrow range of mean Ce anomaly values in both calcites and dolomites (Table 4). However, the calcites have slightly higher mean Ce anomaly values (C1 = 0.90 ± 0.07, *n* = 18 and C3 = 0.94 ± 0.15, *n* = 9) than those of dolomites (D1 = 0.93 ± 0.10, *n* = 19, D2 = 0.80 ± 0.07, *n* = 11, and D3 = 0.87 ± 0.13, *n* = 26). Similarly, the mean Eu anomaly values (Table 4) are higher in calcites (C1 = 1.30 ± 0.51, *n* = 18 and C3 = 1.34 ± 0.51, *n* = 9) than in dolomites (D1 = 1.13 ± 0.23, *n* = 19, D2 = 0.93 ± 0.20, *n* = 11, and D3 = 1.17 ± 0.30, *n* = 26). However, C3 has the highest value, whereas D2 has the lowest of both Ce and Eu anomalies. There are no distinctions in the La anomaly values of both calcite and dolomite generations (Table 4). Except for D2 that has an Eu anomaly slightly below unity (0.93±0.2, *n* = 11), the other carbonate generations that are slightly above unity (Table 4).

Table 4. Summary of statistics of Ce (Ce/Ce*)$_{SN}$, Eu (Eu/Eu*)$_{SN}$ and La (Pr/Pr*)$_{SN}$ anomalies based on the equations of Bau and Dulski (1996).

Phase		Ce^*_{SN} anomaly	Eu^*_{SN} anomaly	La^*_{SN} anomaly
D1	*n*	19	19	19
	Mean	0.93	1.13	1.04
	S.D.	0.10	0.23	0.05
	Max	1.06	1.58	1.11
	Min	0.69	0.45	0.94
D2	*n*	11	11	11
	Mean	0.80	0.93	1.07
	S.D.	0.07	0.20	0.05
	Max	0.96	1.12	1.16
	Min	0.68	0.52	0.99
D3	*n*	26	25	26
	Mean	0.87	1.17	1.07
	S.D.	0.13	0.30	0.08
	Max	1.30	1.88	1.29
	Min	0.50	0.56	0.93
C1	*n*	18	18	18
	Mean	0.90	1.30	1.04
	S.D.	0.07	0.51	0.06
	Max	1.05	2.40	1.15
	Min	0.79	0.50	0.89
C3	*n*	9	9	9
	Mean	0.94	1.34	1.06
	S.D.	0.15	0.51	0.09
	Max	1.23	2.56	1.16
	Min	0.73	0.95	0.88

4.6. Fluid-inclusion gas

Results of fluid inclusion gas analysis of investigated carbonates are presented in Appendix 3. The statistics of CO_2/CH_4, N_2/Ar and Ar/He ratios of weighted mean values of þuid-inclusion gas are shown in Table 5. The ratio of CO_2/CH_4 varied from 4.25 to 122.21 in C1, from 7.41 to

43.20 in D1, from 1.90 to 6.23 in D2, and from 8.31 to 74.90 in D3. The ratio of Ar/He varied from 4.86 to 123.57 in C1, from 1.35 to 7.73 in D1, from 1.21 to 10.14 in D2, and from 0.51 to 15.82 in D3. The ratio of N_2/Ar varied from 68.41 to 118.80 in C1, from 50.13 to 109.72 in D1, from 61.61 to 80.41 in D2, and from 79.29 to 136.32 in D3.

Table 5. Summary of quantitative þuid-inclusion gas analyses (in mol %) using a burst-size weighted mean of several replicate analyses from the investigated samples.

Sample	CO_2	CH_4	Ar	He	N_2	CO_2/CH_4	Ar/He	N_2/Ar
AR5-C1	12.645	2.110	0.031	0.005	2.141	5.99	6.66	68.41
AR5-C1	11.686	2.752	0.018	0.004	1.433	4.25	4.86	79.59
PE4-C1	4.300	0.035	0.024	0.000	2.209	122.21	123.57	92.15
PE5-C1	0.764	0.059	0.001	0.000	0.061	12.89	13.12	118.80
PE5-C1	0.728	0.071	0.002	0.000	0.149	10.32	17.00	87.76
Ar5-D1	15.220	2.054	0.025	0.003	1.259	7.41	7.73	50.13
AR7-D1	10.277	0.950	0.014	0.002	0.855	10.82	7.34	59.22
ES1-D1	11.718	0.271	0.004	0.003	0.411	43.20	1.35	109.72
BR-D2	1.478	0.622	0.002	0.002	0.142	2.38	1.21	61.61
BR2-D2	2.128	1.118	0.004	0.003	0.339	1.90	1.38	80.41
BR3-D2	2.733	0.438	0.021	0.002	1.376	6.23	10.14	66.23
ES1-D3	2.539	0.052	0.002	0.002	0.173	49.12	0.78	96.22
ES1-D3	10.286	0.137	0.005	0.007	0.530	74.90	0.72	109.76
PE1-D3	2.096	0.088	0.017	0.001	1.918	23.95	15.82	110.09
PE14-D3	6.047	0.607	0.010	0.007	0.964	9.95	1.39	99.09
PE3-D3	3.993	0.116	0.001	0.000	0.093	34.31	9.00	103.00
PE3-D3	1.465	0.176	0.003	0.002	0.261	8.31	1.10	101.04
PE4-D3	1.316	0.075	0.003	0.001	0.226	17.54	3.43	79.29
PE5-D3	1.939	0.138	0.002	0.001	0.172	14.07	2.09	100.88
PE5-D3	1.270	0.074	0.004	0.001	0.399	17.14	4.59	96.70
PE13-D3	1.408	0.099	0.001	0.001	0.113	14.26	1.06	95.70
PE15-D3	1.752	0.163	0.001	0.001	0.085	10.73	0.51	136.32

4.7. Halogens

Table 6 shows the results of the halogen contents and F/Cl, Cl/Br and Br/Cl molar ratios of the investigated Esino and Breno carbonates. All of the dolomite generations have similar F/Cl molar ratios (D1, 0.009 to 0.042; D2, 0.010 to 0.023; D3, 0.006 to 0.060). The F/Cl molar ratios are slightly higher in C1 and C3 (0.017 to 0.052 and 0.014 to 0.068, respectively) than those of dolomites, and C3 has the highest value of F/Cl molar ratio. D2 has the narrowest range of Cl/Br ratios (1548 to 2795) and D1 has the highest Cl/Br molar ratios, which are slightly higher than those of D3. C3 has high Cl/Br molar ratios (398 to > 4432) close to those of D1 but C1 has lowest ratios (73 ~ 257), which are dramatically lower than those of C3 and dolomites.

Table 6. Results of the halogen contents and F/Cl and Cl/Br molar ratios of the investigated Esino and Breno carbonates.

Analyte Symbol	F	Cl	Br	F/Cl	Cl/Br
Unit Symbol	mg/L	mg/L	mg/L	(Molar)	(Molar)
Detection Limit	0.01	0.03	0.03		
AR5-D1	0.49	60.9	< 0.03	0.015	> 4575
AR7-D1	0.29	58.5	0.1	0.009	1318
ES1-D1	0.28	17.6	< 0.03	0.030	> 1322
PE8-D1	0.20	8.8	0.05	0.042	398
ES-D2	0.64	124.0	0.1	0.010	2794
BR3-D2	0.25	20.6	< 0.03	0.023	> 1547
AR4-D3	0.23	44.7	< 0.03	0.010	> 3358
ES1-D3	0.98	48.6	0.23	0.038	476
PE5-D3	0.92	79.0	0.23	0.022	774
PE8-D3	0.20	19.9	< 0.03	0.019	> 1495
PE9-D3	0.77	24.1	0.33	0.060	164
PE15-D3	0.10	33.6	0.31	0.006	244
PE9-C1	0.09	10.0	0.31	0.017	72
PE14-C1	0.18	13.7	0.12	0.025	257
PE15-C1	0.39	14.1	0.15	0.052	211
AR4-C3	0.24	31.8	0.18	0.014	398

PG1-C3	2.16	59.0	< 0.03	0.068	> 4432

5. Discussion

5.1. Dolomite petrography

The near micritic grain size (3 - 35ε m), fabric-retention and dull to non-CL exhibited by D1 imply early dolomitization of limemud in shallow burial settings at near-surface conditions, which is consistent with the crosscutting microstylolites. This is also supported by the limited recrystallization in C1, which suggests that the limemud was not exposed to extensive meteoric alteration before dolomitization (e.g., Azmy et al., 2008, 2009) and by the relatively enriched $\delta^{18}O$ values of D1 (-5.9 ± 3.3ă , VPDB) compared with their counterparts of D2 and D3 (Table 2). Also, the lack of evaporite layers reflects dolomitization by diagenetic fluids that were possibly modified seawater or a mixture of meteoric and marine waters (e.g., Hein et al., 1992; Azmy et al., 2008, 2009; Olanipekun, 2014) rather than by evaporated brines. On the other hand, the larger crystal sizes (30 - 600ε m) of D2, relative to that of D1, and fabric destructive textures as well as the high mean T_h value (108 ± 9 °C, n = 58) suggest formation at a later stage of replacement in relatively deeper burial environment and higher temperature than D1. Some of D2 crystals show cloudy core with clear rims indicating replacement of a precursor carbonate (cloudy core) followed by later cementation as a clear rim (e.g., Olanipekum et al., 2014). Earlier studies suggested that similar types of dolomite (D2) could be formed from direct replacement of C1 and C2 or recrystallization of D1 (e.g., Azmy et al., 2008, 2009; Conliffe et al., 2009; Azomani et al., 2013; Olanipekun et al., 2014). No visual porosity has been found in association with D2 in the Esino and Breno carbonates. The latest saddle dolomite D3 generation is limited

to filling vugs and late fractures that cut through all earlier dolomite phases, which implies formation at the deepest diagenetic settings during progressive burial and this is also consistent with the high mean T_h value (111 ± 14 °C， n = 108). The undulose extinction in D3 is the evidence of distorted crystal lattice caused by crystal growth at high temperatures (> 60 °C) of deep burial settings (e.g., Warren, 2000; Rameil, 2008). The zoned CL images of D2 and D3 reþect variations of the chemical composition of diagenetic fluids, particularly Fe and Mn contents, during the course of precipitation (Warren, 2000; Boggs and Krinsley, 2006; Lonnee and Machel, 2006; Heira-Ardakan et al., 2013; Olanipekun et al., 2014).

5.2. Major and minor elements

The molar ratio of Mg and Ca in D1 (Mg/Ca = 43.6/56.4, Table 2) and low Sr concentrations (76 ± 37 ppm) support an early stage of dolomitization of shallow burial environment (Sr < 550 ppm; Tucker and Wright, 1990). The low Sr concentrations of D1 do not support a bacterial origin, as typical for ñprotodolomiteò in sabkhas (Sr > 550 ppm, Tucker and Wright, 1990; Sánchez-Román et al., 2011; Azmy et al., 2013) but may suggest that the parent dolomitizing fluid was diluted with meteoric water (e.g., Sperber et al., 1984; Azmy et al., 2008; 2009, Azomani et al., 2013; Olanipekun et al., 2014), which is consistent with the absence of evaporite layers and sulfate inclusions (e.g., Celestine) in the investigated rocks. The Sr concentration is depleted with progressive diagenesis (Veizer et al., 1983) and the investigated dolomites have generally lower Sr contents than their precursor carbonate (C1), which reflects the influence of diagenetic alteration (Table 2). On the other hand, the Sr concentrations are generally lower in volcanic rocks than in marine carbonates (c.f. Veizer, 1983; Faure, 2001). Therefore, the contribution from the interaction of dolomitizing fluids with the co-occurring volcaniclastic lenses would

unlikely overprint the Sr signature of the dolomites or their precursor limestones, particularly when Sr is depleted with diagenesis (progressive burial). The Breno and Esino lime mudstones were deposited around the late middle Triassic to early late Triassic (Brusca et al, 1981; Berra et al., 2011) likely in aragonitic seas (Dickson, 2004; Hardie, 1996; Sandberg, 1983). The Sr contents of aragonite vary between 6000 ppm and up to 10000 ppm (Veizer, 1983), which is significantly higher than that of calcite (up to ~1000 ppm, Veizer, 1983). If D1 (dolomicrites) inherited its Sr from the precursor lime mudstone, the loss of Sr during diagenesisto the levels of D1 (76 ± 37 ppm) would require extensive alteration including significant meteoric diagenesis and recrystallization (aggrading neomorphism) before dolomitization, although the near-micritic size and fabric preservation of C1 and D1 argues against any significant recrystallization of C1 before and after dolomitization. However, the low partitioning coefficient of Sr in dolomites is likely responsible for the low concentrations of Sr (Land, 1980; Sánchez-Román et al., 2011; Vahrenkamp and Swart, 1990), which is more plausible particularly when the precursor lime muds were precipitated from aragonitic seas. Thus, the precursor (C1) of the investigated dolomicrites (D1) was possibly aragonite although this does not exclude possible contributions from calcite. On the other hand, earlier studies indicated that biomediated (microbial) dolomites may have Sr contents > 1000 ppm (Sánchez-Román et al., 2011), which does not support a microbial origin for the currently investigated dolomicrites (D1).

Iron (Fe) and Mn concentrations reflect the redox conditions in the diagenetic environment (e.g., Veizer, 1983; Tucker and Wright, 1990). Therefore, dolomicrites tend to have low Fe and Mn contents within few hundred ppm due to formation at near-surface/shallow burial conditions (e.g., Azmy et al., 2008, 2009; Azomani et al., 2013; Olanipekun et al., 2014) but carbonates of deep burial diagenesis tend to be enriched in Fe and Mn (Veizer, 1983). However, D1

(dolomicrite) has significantly higher concentrations of Fe (4438 ± 4394 ppm) and Mn (1219 ± 1418 ppm) relative to those of their precursor C1 and even the later dolomite generation D2 (Table 2). The lack of Fe-rich sediments in the succession and the visual estimates of abundance of bacterial microrhombic pyrite in D1 being < 1%, suggest that the parental dolomitizing fluid interacted with volcaniclastic lenses before the dolomitization of calcites so that the fluids became highly enriched with Fe and Mn and/or the dolomitizing basinal fluids of D1 had possibly some contributions from fluids associated with the volcanic activity in the surrounding area (e.g., Hein et al., 1992). Thus, D1 is unlikely to be the precursor of D2 due to the lower Fe and Mn concentrations in D2 (Table 2; 1460 ± 900 ppm and 556 ± 289 ppm, respectively). However, the increase in Fe and Mn from D2 to D3 (1091 ± 1183 ppm and 4463 ± 4888 ppm, respectively) and the trend from C1 to C3 (Table 2), is consistent with the concept of increasing diagenesis with progressive burial (e.g., Veizer et al., 1983; Azmy et al., 2001). Equally, D3 and C3 precipitated from hot basinal fluids that were circulated and interacted with volcaniclastic and other sediments of the basin, and heated with progressive burial.

5.3. Carbon and oxygen isotopes

Despite the diagenetic alteration, both dolomites and calcites have ŭ^{13}C values within the range of the documented signatures of the best preserved Triassic carbonates (Fig. 7; Korte et al., 2005). The poor correlation (R^2 Ò0.3) between Mn/Sr and ŭ^{13}C values (Fig. 8), also suggests that the ŭ^{13}C of diagenetic fluids was likely buffered by that of the surrounding carbonates and that the bituminous material around the growth zones of D2 (Fig. 3) was introduced to the basin of deposition after or at a very late stage of D2 precipitation and before D3. The similar ŭ^{13}C values of C1, D1 and D2 (Table 2) suggest that C1 was likely the precursor of dolomite D1 and D2,

which is supported by the petrographic evidence. On the other hand, the ŭ^{18}O values of both dolomites and calcites are more depleted than those of well-preserved Triassic carbonates (Veizer et al., 1999; Korte et al., 2005), reflecting the influence of water/rock interaction, the initial ŭ^{18}O of the dolomitizing fluids, and temperature of the burial environments (Fig. 7).

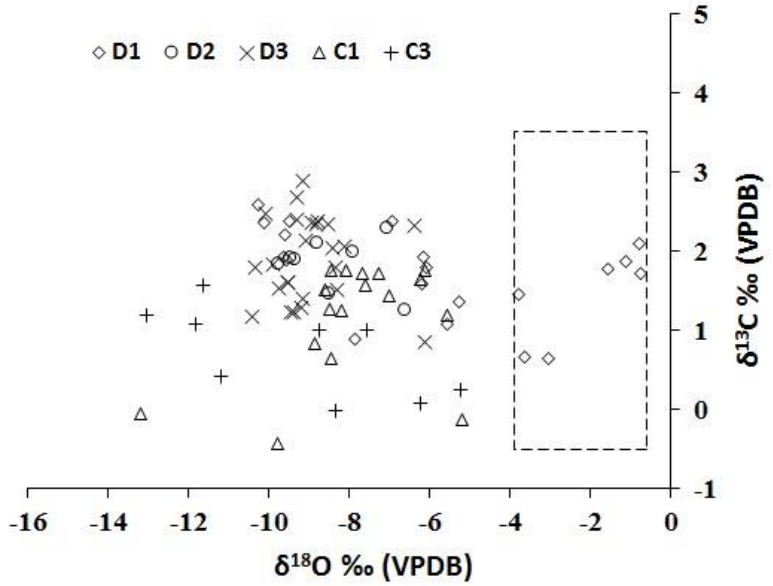

Fig. 7. Scatter diagram of ŭ^{18}O vs. ŭ^{13}C of the investigated carbonates. The square marks the ŭ^{18}O and ŭ^{13}C ranges of composition of the well-preserved Triassic carbonates (Korte et al., 2005).

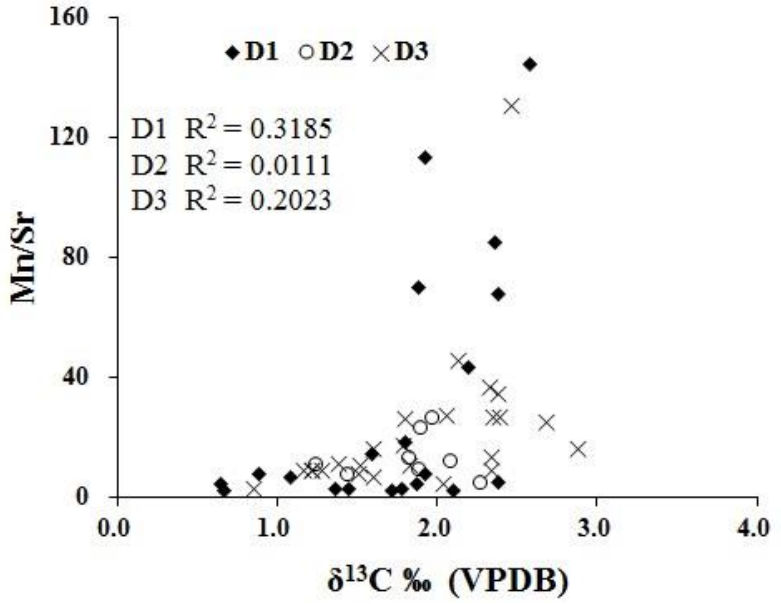

Fig. 8. Scatter diagrams of ŭ^{13}C vs. Mn/Sr of all of the investigated dolomites.

Dolomitization requires large amounts of Mg-rich fluids and the ŭ^{18}O composition of the produced dolomites are therefore dominantly influenced by that of the parent fluid and the temperature of dolomitization. Thus, the ŭ^{18}O of the dolomitizing fluid (Land, 1983) can be calculated by using the T_h values (estimates of minimum entrapment temperature) of primary two-phase fluid inclusions (Goldstein and Reynolds, 1994) and nature of rock fabric, such as grain size (e.g., Azomani et al., 2013; Olanipekun et al., 2014).

The fabric retention and near-micritic grain size of D1 suggest that dolomitization occurred at shallow burial settings of near-surface conditions (T < 50 ºC, Goldstein and Reynolds, 1994). Thus, the ŭ^{18}O (VPDB) of D1 (-10.2 to -0.8ă VPDB; Table 2) imply a parent dolomitizing fluid with ŭ^{18}O approximately between -12.4 and -1.3ă SMOW (Fig. 9). The estimated ŭ^{18}O value of Triassic seawater is between -1 and -4ă SMOW (Veizer et al., 1999; Korte et al., 2005). The investigated sediments reflect precipitation under tropical conditions (e.g., Assereto and Casati,

1965; Berra and Jadoul, 2002; Berra et al., 2011). Assuming that the difference in ŭ^{18}O compositions between the Triassic meteoric and seawaters was similar to that of our modern environment, which is ~ 4ă (Clark and Fritz, 1997), and that the temperature of dolomitization was between 25 to 30 ºC, the calculated ŭ^{18}O value of the Middle Triassic meteoric water is as low as ~ -8ă SMOW and that of the lower end-member value of the D1 parent fluid (~ -12ă SMOW; Fig. 9) is lower than that of meteoric water, which is implausible. This suggests dolomitization at slightly warmer near-surface temperature (45 - 50 ºC; Fig. 9) likely in a mixing zone. Alternatively, the precursor calcite was significantly altered before dolomitization but the fabric retention and near-micritic grain size would argue against repeated meteoric alteration. On the other hand, if dolomitization occurred at 45 - 50 ºC, the ŭ^{18}O of the parent fluid would be between ~ -8 to +3ă SMOW, which is more plausible.

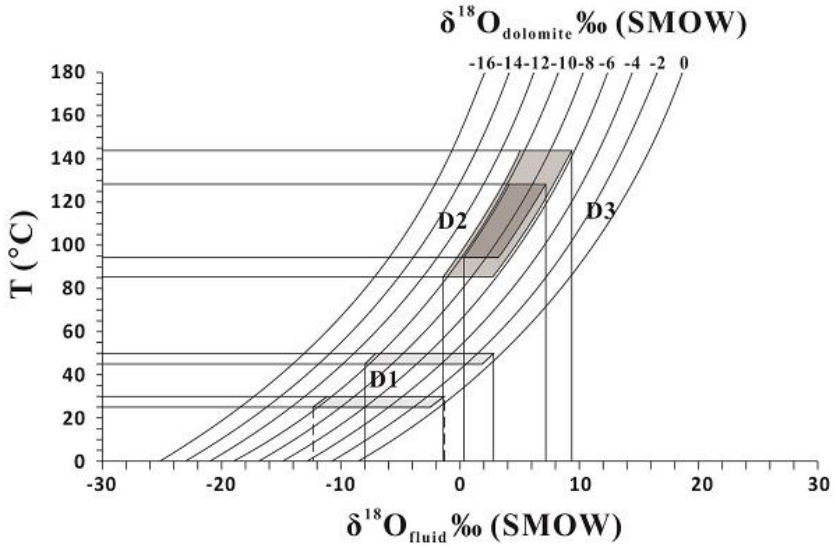

Fig. 9. Temperature (*T*) vs. ŭ^{18}O $_{\text{dagenetic þuid}}$. ŭ^{18}O $_{\text{dolomite}}$ values reconstructed following the equation of Land, 1983 ($10^3 \ln Ŭ = 3.2\times10^6 T^{-2} - 3.3$). The shaded areas indicate the ranges of

ŭ$^{18}O_{\text{þuid}}$ based on the ŭ$^{18}O_{\text{dolomite}}$ values and homogenization temperatures (T_h) of each dolomite generation.

The calculated ŭ^{18}O composition of the parental dolomitizing fluids of D2 and D3 (about 0.4 to 7.1 and -1.5 to 9.4ă SMOW, respectively) is higher than that of D1 (Fig. 9), which is expected for diagenetic fluids at higher temperatures of deeper burial settings since deep basinal brines are more saline and enriched in ^{18}O regardless the age of rocks or location of basins (Goldstein and Reynolds 1994; Azmy et al., 2001; Lonnee and Machel, 2006; Azomani et al., 2013; Haeri-Ardakani et al., 2013; Olanipekun et al., 2014). The high T_h and salinity values of D2 and D3 (Table 1), along with the calculated ŭ^{18}O estimates of their parent fluids (Fig. 9), support an origin from hot basinal fluids that were possibly hydrothermal. Also, the overlap in the ŭ^{18}O of D2 and D3 fluids (Fig. 9) suggests that those dolomites developed from fluids of similar isotopic compositions that possibly evolved through basinal circulation. A similar overlap has been documented in earlier studies of hydrothermal dolomites in other basins (e.g., Azmy et al., 2009; Azomani et al., 2013, Olanipekun et al., 2014).

5.4. Rare earth elements (REE)

The rare earth elements (REE) have been increasingly used as proxies to understand the controls on carbonate diagenesis and identify the origin of diagenetic fluids (e.g., Azmy et al., 2011; Azomani et al., 2013; Haeri-Ardakani et al., 2013). The suite of REE consists of 15 lanthanides (Alibo and Nozaki, 1999), which are classified into light (LREE; La to Nd), medium (MREE: Sm to Dy) and heavy rare earth elements (HREE; Ho to Lu). They are all trivalent except for Ce^{4+} and Eu^{2+} (in some environments) and have similar ionic radii but their chemical characteristics change systematically along the series (Sholkovitz and Shen, 1995). REEs were

incorporated in calcite by substituting for Ca^{2+}, and the distribution pattern of REEs in calcites remains unchanged unless mineral dissolution caused by intense water-rock interaction occurs (Zhong and Mucci, 1995). Therefore, variation of the distribution pattern of REEs in dolomites conveys the information of diagenetic fluid compositions. Ce is sensitive to redox conditions (Sholkovitz et al., 1994) and Eu is known to be more enriched in volcanic rocks relative to sedimentary carbonates (Elderfield and Greaves, 1982). Some recent studies (e.g., Banner et al., 1988; Barton et al., 2006; Webb and Kamber, 2000; Kamber and Webb, 2001; Nothdurft et al., 2004; Webb et al., 2009) suggested that diagenesis, particularly by meteoric and mixed waters, has no significant effect on the pattern, composition and/or distribution of REEs in carbonates (limestones and dolomites) except in systems with extremely high water-rock ratios. In other words, unless there are large amounts of diagenetic fluids to flush the system several times through intense water-rock interaction (i.e., high water-rock interaction ratio), diagenesis has no significant effect on the composition and distribution of REEs in carbonates (limestones and dolomites).

The shale normalized REE patterns of the investigated dolomites (Fig. 6) and the similarity of Ce and La anomalies of dolomites to those of C1 (Fig. 10) show that they may still retain, to some extent, a remnant of the negative Ce anomaly that characterizes the modern brachiopods and also the well-preserved shallow water marine carbonates of the Paleozoic (Azmy et al., 2011). The REE normalized patterns of seawater and shallow-water marine carbonates do not have this Eu anomaly (e.g., Elderfield and Greaves, 1982; Hongo and Nozaki, 2001; Bau et al., 2010). However, the investigated dolomites and calcites contain a slightly positive (>1) Eu anomaly (Fig. 6 and Table 4). A positive Eu anomaly has been documented by earlier studies in fluids from hydrothermal vents at the seafloor and from associated bivalve shells (Bau et al., 2010).

This is consistent with the unusual high Fe contents in D1 and the suggested interaction of the dolomitizing fluid with volcaniclastic lenses prior to dolomitization. Also, the occurrence of slight positive Eu anomaly (Table 4) in C1 suggests that despite the insignificant early meteoric diagenesis of the lime mudstone, it still shows the influence by the volcanic activity in the region, which is expected due to the high sensitivity of REE to diagenesis even when minor (Azmy et al., 2011, 2013). The same effect in D3 and C3 also implies that they were formed from the same earlier basinal fluids that were circulated in the basinal deposits with progressive burial. This also agrees with the parallel shale-normalized trends of all of the investigated carbonates (Fig. 6), thus suggesting that the REE composition of the diagenetic dolomites is, to some extent, controlled by that of the precursor carbonate (e.g., Azomani et al., 2013). However, some of the D2 samples exhibit an Eu anomaly <1 (Tables 3 and 4; Fig. 6), which suggests that the REE composition of its parent diagenetic fluid might have had insignificant influence by the volcanic lenses possibly due to possible temporary restricted fluid circulations caused by changes in tectonic settings in the basin (e.g., Sibson, 1977; Horbury and Robinson, 1993) around the time of formation of D2.

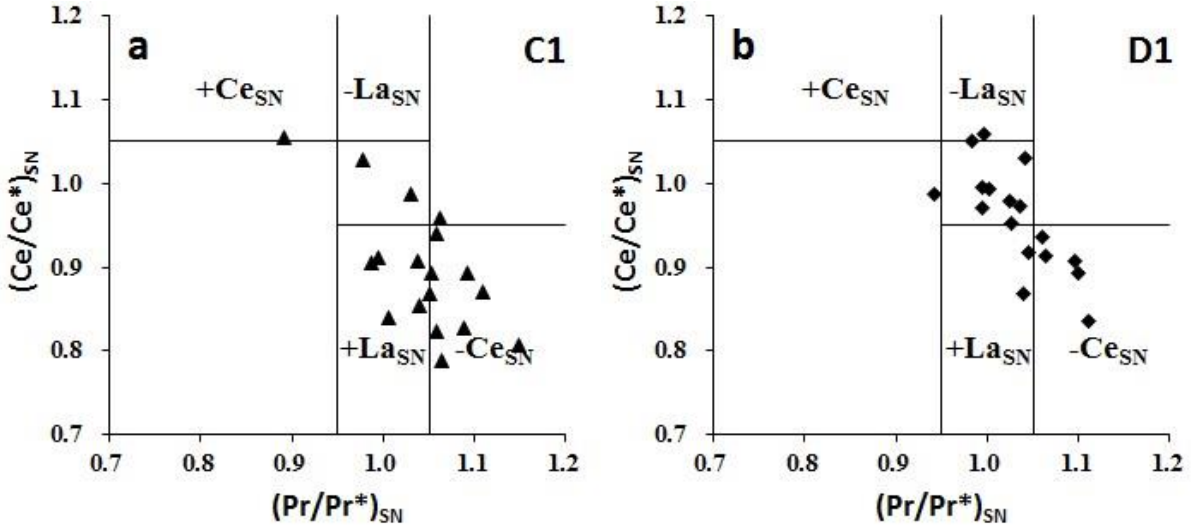

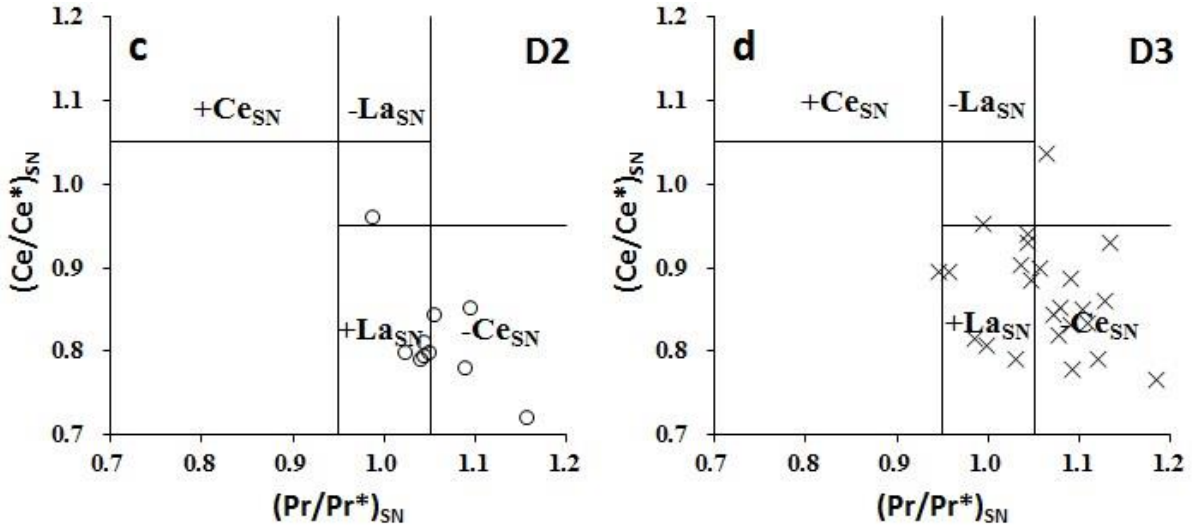

Fig. 10. Scatter diagram of $(Ce/Ce^*)_{SN}$ vs $(Pr/Pr^*)_{SN}$ for the precursor lime mudstone (C1) and all of the investigated dolomites (after Bau and Dulski, 1996).

5.5. Fluid-inclusion gas

The trapped gases in þuid inclusions (Table 5) provide valuable clues of the origin of diagenetic fluids and the oxidation state of diagenetic environments (e.g., Giggenbach, 1986; Norman and Moore, 1999; Blamey and Norman, 2002; Azmy et al., 2013). Giggenbach (1986) introduced the N_2-Ar-He ratios to identify the sources of volatiles in geothermal fluids and attributed high N_2/Ar to magmatic sources. However, Norman and Moore (1999) pointed out that organic nitrogen may also contribute N_2 to increase the N_2/Ar ratio, and thus introduced a CO_2/CH_4 ratio as a proxy since CH_4 reflects the crustal components in thermal fluids and is easy to be analyzed. Norman and Moore (1999) also established the correlation of CO_2/CH_4 with N_2/Ar ratios to identify fluids bearing significant organic nitrogen, which could lead to errors in interpretation. This correlation allows the classification of source fluids into magmatic, meteoric and crustal fluids. Meteoric fluids are near-surface recharge waters whereas crustal fluids can be sourced

from meteoric fluids, but have subsequently interacted with crustal rocks and may have species derived from the wall rock. The CO_2/CH_4 ratios reflect the redox state and their N_2/Ar counterparts are proxies of fluid source(s).

Blamey and Norman (2002) introduced the Ar/He vs. N_2/Ar diagram as a better method to remedy a weakness of the CO_2/CH_4 vs. N_2/Ar diagram, which assumed that most methane is sedimentary in origin but neglected the fact that methane may be produced by inorganic processes.

Figure 11a shows that some of the data points from each investigated carbonate generation (calcites and dolomites) plots within the magmatic zone and along the boundary of the magmatic zone with other zones. However, D2 plots within the evolved crust zone although very close to the boundary of the magmatic zone. This suggests a possible contribution of fluids from volcanic activity to the parental diagenetic fluids of the dolomites and calcites. However, except for the co-occurring volcaniclastic lenses, the investigated sequence of dolomites and the close neighborhood sediments do not have a clear filed evidence of a specific type of volcanic activity (e.g., sill, dyke, hydrothermal vent or flank flux) directly related the dolomitization events, which makes the interpretation of the exact origin of those volcanic fluids very difficult and the interpretation of the fluid-inclusion gas ratios, particularly the few data points that plot within the magmatic zone (Fig. 11a, b), have to be taken with cautions due to the lack of supporting field evidence. On the other hand, the major occurrence of points along or close to the boundary of the magmatic zones suggests that the contribution from those volcanic fluids was most likely restricted or insignificant and that the diagenetic fluid composition was mainly buffered by that of the basinal fluids and evolved through circulation with progressive burial. Similarly, Figure

11b shows few data points located along or close to the boundary of the magmatic zone, which is consistent with the suggested scenario of buffering diagenetic fluids with progressive burial. Also, the investigated dolomites are not expected to plot entirely within the calc-alkaline magmatic since they are not magmatic rocks but were formed by basinal diagenetic fluids.

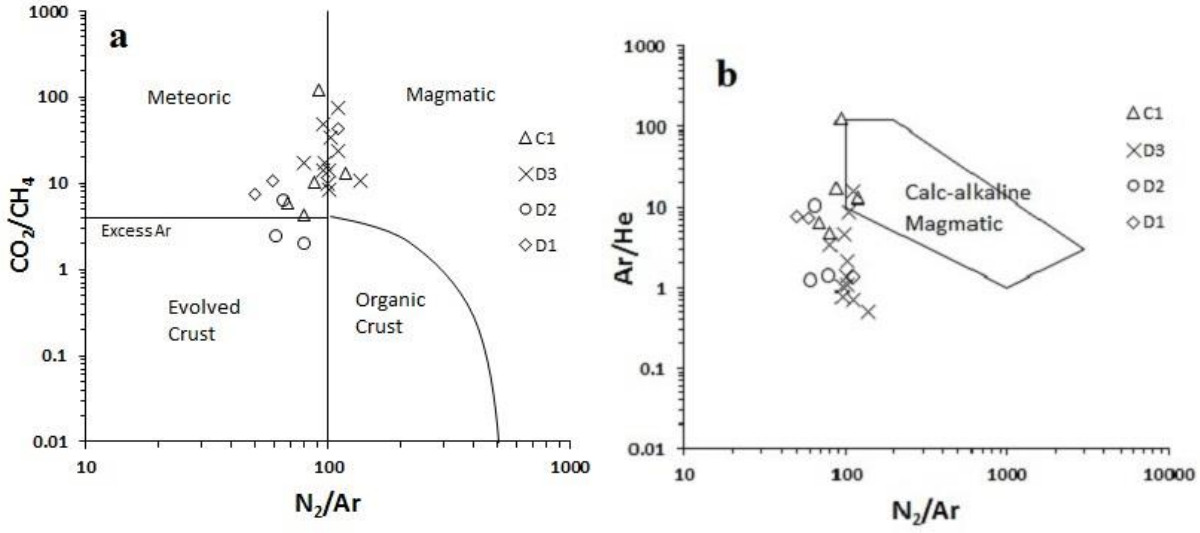

Fig. 11. Scatter diagrams of (a) N_2/Ar vs. CO_2/CH_4 and (b) N_2/Ar vs. Ar/He for C1 and dolomites (D1, D2, and D3) of the Esino and Breno formations (after Norman and Moore, 1999; Blamey and Norman, 2002; Blamey, 2012) based on the weighted mean values (Appendix 3).

5.6. Halogens

The halogens contents of fluid inclusions (Table 6) are useful in providing information about the diagenetic environment and the sources of dolomitizing fluids (Banks et al., 2002; Gleeson and Turner, 2007; Conliffe et al., 2010). The F/Cl molar ratios of the fluid inclusions of calcites and dolomites of the Esino and Breno formations are within the range of ultramafic and mafic rocks (< 0.016 ~ 0.044, Orberger et al., 1990) but much greater than that of seawater (0.1×10^{-3}, Wilson,

1975). Based on Hanorôs (1994) classification of the subsurface saline waters in sedimentary basins, the salinities of D2, D3 and C3 diagenetic fluids (23 ± 2 eq wt% NaCl, *n* = 44, 20 ± 4 eq wt% NaCl, *n* = 104, and 22 ± 5 eq wt% NaCl, *n* = 63, respectively) indicate that they are Cl^--dominated and halite-undersaturated saline waters. Therefore, the high F/Cl molar ratios in the fluid inclusions of calcites and dolomites are likely caused by high F^- rather than lower Cl^-. Thus, the high F^- concentrations and high F/Cl molar ratios were likely derived from the water-rock interaction of the diagenetic fluids with the volcaniclastic lenses.

The fluid inclusions in dolomite generations and C3 show higher Cl/Br molar ratios than that of seawater (648, Wilson, 1975; 653, Jambon et al., 1995), and MORB (969, Jambon et al., 1995) and most Cl/Br molar ratios of dolomite generations and C3 (D1, 398 to > 4575; D2, 1547 to 2794; D3, 164 to > 3358; C3, 398 to > 4432) fall within the ranges of seawater (648, Wilson, 1975), ultramafic and mafic rocks (188 to ~1428, Orberger et al.,1990) and magmatic fluids (1492 to ~ 8333, Banks et al., 2000). Since there are no evaporite layers in the investigated rocks, which is supported by evidence of mineral texture and Sr concentrations, high Cl/Br molar ratios likely reflect the water-rock interaction of the diagenetic fluids with the volcaniclastic rocks (lenses). Low Cl/Br (72 ج 257) molar ratio of C1 (and a few other dolomite samples) might be the result of dilution of their parent diagenetic fluids with meteoric water.

The multi-technique approach has proven an efficient tool in understanding the origin of dolomites. The geochemical signatures retained by dolomites of the Esino and Breno formations, including petrography, microthermometry, fluid-inclusion gas ratios, stable isotopes, minor and REE, and halogens are consistent and reflect the impact of the co-occurring volcaniclastic lenses. They also allow better understanding the origin and nature of the parental dolomitizing fluids in the basin.

6. Conclusions

Petrographic examination of carbonates of the Esino and Breno formations in the western Southern Alps reveals three main non-porous generations of dolomites: an early replacive dolomicrite (D1), later larger replacive eu- to subhedral dolomite (D2) and latest coarse sub- to anhedral fracture-ýlling saddle dolomite (D3).

Petrographic characteristics of dolomite D1 suggest an early dolomitization event under relatively shallow burial environment at near-surface conditions. The high Fe and Mn contents and ^{18}O enriched estimates of the parental dolomitizing fluids suggest that D1 originated at early stage of diagenesis of shallow burial setting at near-surface conditions (40 - 50 ºC).

Microthermometric analyses of fluid inclusions trapped within D2 and D3 mineral crystals and elemental geochemistry suggest that D2 and D3 were formed during later stages of diagenesis under deeper burial settings from hot fluids with high salinities, which is supported by the calculated ŭ^{18}O composition of their parent dolomitizing fluids.

The REE compositions and similarity of shale-normalized patterns of investigated generations of dolomites suggest that they likely developed from comparable basinal diagenetic fluids that their composition evolved during progressive burial. The positive Eu anomaly of the investigated dolomites shows the influence of the reaction of dolomitizing fluids with the associated volcaniclastic lenses prior to dolomitization.

Fluid-inclusion gas analyses also support some contributions, possibly limited, of fluids related to volcanic activities to the parent diagenetic fluids of all dolomites and calcites. Furthermore, the high F contents, high F/Cl and high Cl/Br molar ratios in the fluid inclusions of the

investigated dolomites reflect the influence of the water-rock interaction of the diagenetic fluids with the volcaniclastic lenses, which is consistent with their geochemistry.

Acknowledgements

The authors wish to thank anonymous reviewers for their constructive and critical reviews. Also, efforts of Dr. Octavian Catuneanu (Editor-in-Chief) and Dr. Nereo Preto (Associate Editor) are much appreciated. This project was supported by funds (to Karem Azmy) from the Petroleum Exploration Enhancement Program (PEEP).

References

Alibo, D.S., Nozaki, Y., 1999. Rare earth elements in seawater: particle association, shale normalization and Ce oxidation. Geochimica et Cosmochimica Acta 63, 363 - 372.

Assereto, R., Brigo, L., Jadoul, F., Omenetto, P., Perna, G., Rodeghiero, F., Vailati, G., 1979. Recent studies on Pb-Zn-Fluorite and Barite deposits in the Mid- and Upper-Triassic series of the Lombardy Prealps: Verh. Geol. BA 1978, 197-204.

Assereto, R., Casati, P., 1965. Revisione della stratigraýa permo-triassica della Val Camonica meridionale (Lombardia). Riv. Ital. Paleontol. Stratigr. 71, 999 - 1097, Milano.

Assereto, R., Folk, R.L., 1980. Diagenetic fabrics of aragonite, calcite and dolomite in ancient peritidal-spelean environment: Triassic Calcare Rosso, Lombardia, Italy. Journal of Sedimentary Petrology 50, 371 - 394.

Assereto, R., Jadoul, F., Omenetto P., 1977. Stratigrafia e metallo genesi del settore occidentale del distretto a Pb, Zn, fluorite e barite di Gorno (Alpi Bergamasche). Riv. It. Paleont. Strat. 83, 395-532, Milano.

Assereto, R., Kendall, C. G. S. C., 1971. Megapolygons in Ladinian limestones of Triassic of Southern Alps: evidence of deformation by penecontemporaneous desiccation and cementation. Journal of Sedimentary Research, 41(3).

Assereto R., Kendall C. G. S. C., 1977. Nature, origin and classification of peritidal tepee structures and relative breccias. Sedimentology 24, 153- 210, Oxford.

Azmy, K., Blamey, N.J.F., 2013. Origin of diagenetic fluids inferred from fluid inclusion gas ratios. Ghemical Geology 347, 246-254.

Azmy, K., Brand, U., Sylvester, P., Gleeson, S., Logan, A., Bitner, M.A., 2011. Biogenic lowï Mg calcite (brachiopods): proxy of seawaterï REE composition, natural processes and diagenetic alteration. Chemical Geology 280, 180-190.

Azmy, K., Knight, I., Lavoie, D. and Chi, G., 2009. Origin of the Boat Harbour dolomites of St. George Group in western Newfoundland, Canada: implications for porosity controls. Bulletin of Canadian Petroleum Geology 57, 81ï 104.

Azmy, K., Lavoie, D., Knight, I. and Chi, G., 2008. Dolomitization of the Aguathuna Formation carbonates of Port au Port Peninsula in western Newfoundland, Canada: implications for a hydrocarbon reservoir. Canadian Journal of Earth Sciences 45, 795ï 813.

Azmy, K., Lavoie, D., Wang, Z., Brand, U., Al-Aasm, I., Jackson, S., Girard, I., 2013. Magnesium-isotope and REE compositions of Lower Ordovician carbonates from eastern Laurentia: implications for the origin of dolomites and limestones. Chemical Geology 356, 64-75.

Azmy, K., Stouge, S., Brand, U., Bagnoli, G., & Ripperdan, R., 2014. High-resolution chemostratigraphy of the Cambrianï Ordovician GSSP: Enhanced global correlation tool. Palaeogeography, Palaeoclimatology, Palaeoecology 409, 135-144.

Azmy, K., Veizer, J., Misi, A., de Oliveira, T. F., Sanches, A. L., Dardenne, M. A., 2001. Dolomitization and isotope stratigraphy of the Vazante Formation, São Francisco Basin, Brazil. Precambrian Research 112(3), 303-329.

Azomani, E., Azmy, K., Blamey, N., Brand, U., Al-Aasm, I., 2013. Origin of Lower Ordovician dolomites in eastern Laurentia: controls on porosity and implications from geochemistry. Marine and Petroleum Geology 40, 99-114.

Banks D. A., Boyce A. J., Samson I. M., 2002. Constraints on the origins of þuids forming Irish Zn-Pb-Ba deposits: evidence from the composition of þuid inclusions. Economic Geology 97, 471-480.

Banks, D. A., Green, R., Cliff, R. A., Yardley, B. W. D., 2000. Chlorine isotopes in fluid inclusions: determination of the origins of salinity in magmatic fluids. Geochimica et Cosmochimica Acta 64, 1785-1789.

Banks, D. A., Yardley, B. W. D., 1992. Crush-leach analysis of fluid inclusions in small natural and synthetic samples. Geochimica et Cosmochimica Acta 56, 245-248.

Banner, J.L., Hanson, G.N., Meyers, W.J., 1988. Rare earth element and Nd isotopic variations in regionally extensive dolomites from the Burlingtonï Keokuk Formation (Mississippian): implications for REE mobility during carbonate diagenesis. Journal of Sedimentary Petrology 58, 415ï 432.

Barton, E.D., Bau, M., Alexander, B., 2006. Preservation of primary REE patterns without Ce anomaly during dolomitization of Mid-Paleoproterozoic limestone and the potential re-establishment of marine anoxia immediately after the óGreat Oxidation Eventô South African Journal of Geology 109, 81ï 86.

Bau, M., Balan, S., Schmidt, K., Koschinsky, A., 2010. Rare earth elements in mussel shells of the Mytilidae family as tracers for hidden and fossil high-temperature hydrothermal systems. Earth and Planetary Science Letters 299(3), 310-316.

Bau, M., Dulski, P., 1996. Distribution of yttrium and rare-earth elements in the Penge and Kuruman iron-formations, Transvaal Supergroup, South Africa. Precambrian Research 79, 37-55.

Bernal, N. F., Gleeson, S. A., Dean, A. S., Liu, X. M., Hoskin, P., 2014. The source of halogens in geothermal fluids from the Taupo Volcanic Zone, North Island, New Zealand. Geochimica et Cosmochimica Acta 126, 265-283.

Berra, F., 2007. Sedimentation in shallow to deep water carbonate environments across a sequence boundary: effects of a fall in sea-level on the evolution of a carbonate system (Ladinian - Carnian, eastern Lombardy, Italy). Sedimentology 54, 721 ï 735.

Berra, F., 2012. Sea-level fall, carbonate production, rainy days: How do they relate? Insight from Triassic carbonate platforms (Western Tethys, Southern Alps, Italy). Geology 40, 271ï 274.

Berra F., Balini M., Levera M., Nicora A. and Salamati R., 2012. Anatomy of carbonate mounds from the Middle Anisian of Nakhlak (Central Iran): architecture and age of a subtidal microbial-bioclastic carbonate factory. Facies 58, 685-705.

Berra, F., Carminati, E., 2010. Subsidence history from a backstripping analysis of the Permo-Mesozoic succession of the Central Southern Alps (Northern Italy). Basin Research 22, 952ï 975

Berra, F., Carminati, E., 2012. Differential compaction and early rock fracturing in high-relief carbonate platforms: numericalmodelling of a Triassic case study (Esino Limestone, Central Southern Alps, Italy). Basin Research 24, 598 ï 614

Berra, F., Jadoul, F., 2002. Sedimentological and paleontological evidences of a ñMid Carnianò transgression in the Western Southern Alps (S. Giovanni Bianco Fm., Lombardy, Italy): stratigraphic and paleogeographic implications. Riv. It. Paleont. Strat. 108, 119-131.

Berra, F., Jadoul, F., Binda, M., Lanfranchi, A., 2011. Large-scale progradation, demise and rebirth of a high relief, þat-topped carbonate factory (Late Anisian-Early Carnian, Lombardy Southern Alps, Italy). Sed. Geol. 23, 48 ï 63.

Bertotti, G., Picotti, V., Bernoulli, D., Castellarin, A., 1993. From rifting to drifting: tectonic evolution of the South-Alpine upper crust from the Triassic to the Early Cretaceous. Sedimentary Geology 86, 53-76.

Blamey, N.J.F., 2012. Composition and evolution of crustal, geothermal and hydrothermal fluids interpreted using quantitative fluid inclusion gas analysis. Journal of Geochemical Exploration 116, 17-27.

Blamey, N.J.F., Norman, D. I., 2002. New Interpretations of Geothermal Fluid Inclusion Volatiles: Ar/He and N2/Ar ratios-A Better Indicator of Magmatic Volatiles, and Equilibrium Gas Geothermometry. In Proceedings: Twenty-seventh Workshop on Geothermal Reservoir Engineering, Stanford University, Stanford, California.

Blamey, N.J.F., Parnell, J., McMahon, S., Mark, D., Tomkinson, T., Lee, M., Shivak, J., Izawa, M., Banerjee, M., Flemming, R., 2015. Evidence for methane in Martian meteorites. Nature Communications 6: 7339, DOI: 10.1038.

Bodnar, R.J., 1993. Revised equation and table for determining the freezing point depression of H2O-NaCl solutions. Geochimica et Cosmochimica Acta 57, 683-684.

Bodnar, R.J., 2003. Interpretation of data from aqueous-electrolyte fluid inclusions. In: Samson, I., Anderson, A., Marshal, D. (Eds.), Fluid Inclusions: Analyses and Interpretation. Short Course Series, vol. 32, Mineralogical Association of Canada, 81 - 100.

Boggs, S., Krinsley, D., 2006. Application of cathodoluminescence imaging to the tudy of sedimentary rocks, New York, Cambridge University Press, 165p.

Bosellini, A., and Rossi, D., 1974a, Triassic carbonate buildups of northern Italy. In: Laporte, L, ed., Reefs in Time and Space: Society of Economic Paleontologists and Mineralogists Special Publication 18, p. 209-233.

Bosellini, A., and Rossi, D., 1974b, Triassic carbonate buildups of northern Italy. American Association of Petroleum Geologists Bulletin, v. 54, p. 836-837.

Bosellini, A, Gianolla, P., and Stefani, M., 2003, Geology of the Dolomites. Episodes, v. 26, no. 3, p. 181-185.

Brusca, C., Gaetani, M., Jadoul, F. Viel, G., 1981. Paleogeografia e metallogenesi del Sudalpino. Mem. Soc. Geol. It. 22, 65-82, Roma.

Castellarin A; Lucchini F; Rossi P L; Simboli G; Bosellini A; Sommavilla E, 1979. Middle Triassic magmatism in Southern Alps. II: a geodynamic model, Rivista italiana di paleontologia e stratigrafia 85, 1111-1124.

Clark, I.D., Fritz, P., 1997. Environmental Isotopes in Hydrogeology. Lewis Publisher, Boca Raton, FL, 328 pp.

Coleman, M.L., Walsh, J.N. and Benmore, R.A., 1989. Determination of both chemical and stable isotope composition in milligram-size carbonate samples. In: B.W. Sellwood (Editor),

Zoned Carbonate Cements: Techniques, Applications and Implications. Sedimentary geology 65, 233-238.

Conliffe, J., Azmy, K., Gleeson, S.A., Lavoie, D., 2010. Fluids associated with hydrothermal dolomitization in St. George Group, western Newfoundland, Canada. Geoþuids 10, 422-437.

Conliffe, J., Azmy, K., Knight, I., Lavoie, D., 2009. Dolomitization of the Lower Ordovician Watts Bight Formation of the St. George Group, western Newfoundland; evidence of hydrothermal þuid alteration. Canadian Journal of Earth Sciences 46, 247-261.

Crisci, C. M., Ferrara, G., Mazzuoli, R., Rossi, P. M., 1984. Geochemical and geochronological data on Triassic volcanism of the Southern Alps of Lombardy (Italy): genetic implications. Geologische Rundschau, 73(1), 279-292.

Dickson, J. A. D., 1966. Carbonate identification and genesis as revealed by staining, Journal of Sedimentary Research, 36(2).

Dickson, J. A. D., 2004. Echinoderm skeletal preservation: calcite-aragonite seas and the Mg/Ca ratio of Phanerozoic oceans. Journal of Sedimentary Research 74(3), 355-365.

Elderfield, H. and Greaves, M.J., 1982. The rare earth elements in seawater. Nature 296, 214 - 219.

Faure, G., 2001. Origin of Igneous Rocks: The Isotopic Evidence. Springer, Verlag, Berlin, Heildelberg. 496p.

Feist-Burkhardt, S., Götz, A.E., Szulc, J., Borkhataria, R., Geluk, M., Haas, J., Hornung, J., Jordan, P., Kempf, O., Michalík, J., Nawrocki, J., Reinhardt, L., Ricken, W., Röhling, H-G., Rüffer, T., Török, Á., Zühlke, R., 2008. Triassic. In: McCann, T. (Ed.), The Geology of Central Europe, Mesozoic and Cenozoic. Geological Society of London 2, 749ï 822.

Gaetani, M., Gnaccolini, M., Jadoul, F., Garzanti, E., 1998. Multiorder sequence stratigraphy in the Triassic system of the Western Southern Alps. In: de Graciansky, P.C., Hardenbol, J., Jacquin, T., Vail, P.R. (Eds.), Mesozoic and Cenozoic Sequence Stratigraphy of European Basins. SEPM Spec. Publ. vol. 60, pp. 701ï 717.

Garzanti, 1985. The sandstone memory of the evolution of a Triassic volcanic arc in the Southern Alps, Italy. Sedimentology 32, 423-433.

Garzanti, E., Gnaccolini, M., Jadoul, F., 1995. Anatomy of a semiarid coastal system: the Upper Carnian of Lombardy (Italy). Riv. It. Paleont. Strat 101(1), 17-36.

Giggenbach, W. F., 1986. "The use of gas chemistry in delineating the origin of fluids discharges over the Taupo Volcanic Zone: A review," International Volcanological Congress, Hamilton, New Zealand. Proceedings Symposium 5, 47-50.

Gleeson S. A., Turner W. A., 2007. Fluid inclusion constraints on the origin of the brines responsible for Pb-Zn mineralization at Pine Point and coarse non-saddle and saddle dolomite formation in southern Northwest Territories. Geoþuids 7, 51ï 68.

Gnaccolini, M., 1983. Un apparato deltizio Triassico nelle Prealpi Bergamasche. Rivista ltaliana di Paleontologia e Stratigrafia 88, 599-612.

Gnaccolini, M., 1986. La Formazione di Gorno nei dintorni di Dossena e di Gorno (Prealpi Bergamasche): analisi di una la- guna triassica. Riv. Ital. Paleont. Strat. 92, 3-32.

Gnaccolini, M., 1988. Arenaria di Val Sabbia e Formazione di Gorno: Un sistema deposizionale delta - laguna nel Trias superiore delle Prealpi Bergamasche. Riv. Ital. Paleont. Strat. 93, 329-336.

Gnaccolini, M., Jadoul, F., 1988. Un sistema deposizionale delta-laguna-piattaforma carbonatica: un esempio del Trias superiore lombardo (Alpi Meridionali). Riv. Ital. Paleont. Strat 93, 10-32.

Gnaccolini, M., Jadoul, F., 1990. Carbonate platform, lagoon and delta "high-frequency" cycles from the Carnian of Lombardy (Southern Alps, Italy). Sedimentary Geology 67, 143-159.

Goldstein, R.H., Reynolds, T.J., 1994. Systematics of Fluid Inclusions in Diagenetic Minerals. Society for Sedimentary Geology (SEPM) Short Course, Tulsa, Okla.

Haeri-Ardakani, O., Al-Aasm, I., Coniglio, M., Samson, I., 2013. Diagenetic evolution and associated mineralization in Middle Devonian carbonates, southwestern Ontario, Canada. Bulletin of Canadian Petroleum Geology 61, 41-58.

Hardie, L. A., 1996. Secular variation in seawater chemistry: An explanation for the coupled secular variation in the mineralogies of marine limestones and potash evaporites over the past 600 m.y. Geology 24(3), 279-283.

Hanor, J. S., 1994. Origin of saline fluids in sedimentary basins. Geological Society, London, Special Publications 78, 151-174.

Hein, J. R., Gray, S. C., Richmond, B. M., White, L. D., 1992. Dolomitization of Quaternary reef limestone, Aitutaki, Cook Islands. Sedimentology 39(4), 645-661.

Hongo, Y., Nozaki, Y., 2001. Rare earth element geochemistry of hydrothermal deposits and Calyptogena shell from the Iheya Ridge vent field, Okinawa Trough. Geochemical Journal-Japan 35(5), 347-354.

Horbury, A.D., Robinson, A.G., 1993. Diagenesis and basin development. AAPG: Studies in Geology, 274p.

Jadoul, F., Gervasutti, M. and Fantini Sestini, N., 1992. The Middle Triassic of the Brembana Valley: preliminary study of the Esino platform (Bergamasc Alps), Riv. Ital. Paleontol. Stratigr. 98, 299-324.

Jadoul, F., Nicora, A., Ortenze, A., Pohar, C., 2002. Ladinian stratigraphy and paleogeography of the Southern Val Canale (Pontebbano-Tarvisiano, Julian Alps, Italy). Soc. Geol. Ital. Mem. 57, 29-43.

Jadoul, F., Rossi, P.M., 1982. Evoluzione paleogeografico-strutturale e vulcanismo triassico nella Lombardia centro-occidentale, In: Guida alla geologia del Sudalpino centrooccidentale, Guide Geol. Reg. S.G.I.: 143-155, Bologna

Jadoul, F., Weissert, H., 1989. Evinosponges in the Triassic Esino Limestone (Southern Alps): documentation of early lithification and late diagenetic overprint. Sedimentology, 36, 685-699.

Jambon, A., Déruelle, B., Dreibus, G., Pineau, F., 1995. Chlorine and bromine abundance in MORB: the contrasting behaviour of the Mid-Atlantic Ridge and East Pacific Rise and implications for chlorine geodynamic cycle. Chemical Geology 126, 101-117.

Kamber, B.S., Webb, G.E., 2001. The geochemistry of late Archean microbial carbonate: implications for ocean chemistry and continental erosion history. Geochimica et Cosmochimica Acta 65, 2509-2525.

Korte, C., Kozur, H. W., Veizer, J., 2005. ŭ^{13}C and ŭ^{18}O values of Triassic brachiopods and carbonate rocks as proxies for coeval seawater and palaeotemperature. Palaeogeography, Palaeoclimatology, Palaeoecology 226, 287-306.

Land, L.S., 1980. The isotopic and trace element geochemistry of dolomite: the state of the art. In: Zenger, D.H., Dunham, J.B., Ethington, R.L. (Eds.), Concepts and Models of Dolomitization: Society of Sedimentary Geology. Special Publications, 87ï 110.

Land, L.S. 1983. The application of stable isotopes to studies of the origin of dolomite and to problems of diagenesis of clastic sediments. In Society for Sedimentary Geology (SEPM) Short Course Notes 10. Edited by M.A. Arthur, T.F. Anderson, I.R. Kaplan, J. Veizer, and L.S. Land. pp. 4.1ï 4.22.

Lawler, J.P., Crawford, M.L., 1983. Stretching of fluid inclusions resulting from a low temperature microthermometric technique. Econ. Geol. 78, 527-529.

Lonnee, J., Machel, H. G., 2006. Pervasive dolomitization with subsequent hydrothermal alteration in the Clarke Lake gas field, Middle Devonian Slave Point Formation, British Columbia, Canada. AAPG Bulletin 90(11), 1739-1761.

McLennan, S.M., 1989. Rare earth elements in sedimentary rocks: inþuence of provenance and sedimentary processes. In: Lipin, B.R., McKay, G.A. (Eds.), Geochemistry and Mineralogy of Rare Earth Elements. Mineral. Soc. Am. Rev. Miner. 21, 169 - 200.

Mutti, M., 1994. Association of tepees and paleokarsts in the Ladinian Calcare Rosso (Southern Alps, Italy). Sedimentology, 41, 621 - 641.

Norman, D.I., Blamey, N.J.F., 2001. Quantitative analysis of fluid inclusion volatiles by a two mass spectrometer system, In: Noronha, F., Doria, A., Guedes, A. (Eds.), European Current Research on Fluid Inclusions, Porto 2001 (XVI ECROFI): Faculdidade de Ciencias do Porto, Departamento de Geologia, Memoria 7, 341 - 344.

Norman, D.I., Moore, J.N., 1997. Gaseous species in fluid inclusions: a fluid tracer and indicator of fluid processes [abs.]: European current research on fluid inclusions, No. XIV, Nancy, France, Abstracts, pp. 243-244.

Norman, D.I., Moore, J.N., 1999. Methane and excess N_2 and Ar in geothermal fluid inclusions. Proceedings: Twenty-fourth workshop of geothermal reservoir engineering, Stanford University, Stanford, California, January 22ï 24, pp. 233ï 240.

Nothdurft, L.D., Webb, G.E., Kamber, B.S., 2004. Rare earth element geochemistry of Late Devonian reefal carbonates, Canning Basin, Western Australia: confirmation of a seawater REE proxy in ancient limestones. Geochimica et Cosmochimica Acta 68, 263ï 283.

Obenholzner, J.H., 1991. Triassic volcanogenic sediments from the Southern Alps (Italy, Austria, Yugoslavia) - a contribution to the "Pietra verde" problem, In: R. Cas and C. Busby-Spera (Editors), Voleaniclastic Sedimentation. Sedimentary Geology 74: 157-171.

Olanipekun, B., Azmy, K., Brand, U., 2014. Dolomites of the Boat Harbour Formation in the Northern Peninsula, western Newfoundland, Canada: Implications for dolomitization history and porosity control. AAPG Bulletin 98, 765ï 791

Orberger, B., Friedrich, G., Woermann, E., 1990. The distribution of halogens and carbon in PGE-bearing ultramafics of the Acoje ophiolite block, Zambales, Philippines. Journal of Geochemical Exploration 37(1), 147-169.

Parry, W.T., Blamey, N.J.F., 2010. Fault þuid composition from þuid inclusion measurements, Laramide age Uinta thrust fault, Utah. Chemical Geology 278, 105 - 119.

Pisa G., Castellarin A., Lucchini F., Rossi P. L., Simboli G., Bosellini A., Sommavilla E., 1979. "Middle Triassic magmatism in southern Alps. I: a review of general data in the Dolomites", Rivista italiana di paleontologia e stratigrafia 85(03-04), 1093-1110.

Rameil, N. 2008. Early diagenetic dolomitization and dedolomitization of Late Jurassic and earliest Cretaceous platform carbonates: a case study from the Jura Mountains (NW Switzerland, E France). Sedimentary Geology 212, 70ï 85.

Ronchi, P., Jadoul, F., Ceriani, A., Di Giulio, A., Scotti, P., Ortenzi, A., Previde Massara, E., 2011. Multistage dolomitization and distribution of dolomitized bodies in Early Jurassic carbonate platforms (Southern Alps, Italy). Sedimentology, 58(2), 532-565.

Sánchez-Román, M., McKenzie, J.A., de Luca Rebello Wagner, A., Romanek, C.S., Sánchez-Navas, A., Vasconcelos, C., 2011. Experimentally determined biomediated Sr partition coefficient for dolomite: significance and implication for natural dolomite. Geochimica et Cosmochimica Acta 75, 887ï 904.

Sandberg, P. A., 1983. An oscillating trend in Phanerozoic nonskeletal carbonate mineralogy. Nature 305, 19 ï 22.

Shepherd, T.J., Rankin, A.H., Alderton, D.H.M., 1985. A Practical Guide to Fluid Inclusions. Blackie, London.

Sholkovitz, E., Landing, W.M., Lewis, B.L., 1994. Ocean particle chemistry: the fractionation of rare earth elements between suspended particles and seawater, Geochimica et Cosmochimica Acta 58, 1576-1580.

Sholkovitz, E., Shen, G.T., 1995. The incorporation of rare-earth elements in modern coral. Geochimica et Cosmochimica Acta 59, 2749-2756.

Sibson, R.H., 1977. Fault rocks and fault mechanisms. Geological Society of London 133, 191-213.

Sperber, C.M., Wilkinson, B.H., Peacor, D.R., 1984. Rock composition, dolomite stoichiometry, and rock/water reactions in dolomitic carbonate rocks. Journal of Geology 92(6), 609-622.

Tucker, M.E., and Wright, V.P., 1990. Carbonate Sedimentology. Blackwell Publishing, Oxford, UK.

Vahrenkamp V. C., Swart P. K., 1990. New distribution coefficient for the incorporation of strontium into dolomite and its implications for the formation of ancient dolomites. Geology 18, 387ï 391.

Veizer, J., 1983. Chemical diagenesis of carbonates: theory and application of trace element technique. In: Arthur, M.A., Anderson, T.F., Kaplan, I.R., Veizer, J., Land, L.S. (Eds.), Stable Isotopes in Sedimentary Geology. Society of Economic Paleontologists and Mineralogists Short Course Notes, 10, pp. III-1ï III-100.

Veizer, J., Ala, D., Azmy, K., Bruckschen, P., Bruhn, F., Buhl, D.,et al. 1999. $^{87}Sr/^{86}Sr$, ŭ^{18}O and ŭ^{13}C evolution of Phanerozoic seawater. Chemical Geology 161, 59-88.

Veizer, J., Compston, W., Clauer, N., Schidlowski, M., 1983. $^{87}Sr/^{86}Sr$ in Late Proterozoic carbonates: evidence for a ñmantleò event at ~ 900 Ma ago. Geochimica et Cosmochimica Acta 47(2), 295-302.

Vola, G., Jadoul, F., 2014. Applied stratigraphy and carbonate petrography of the Arabescato Orobico dimension stone from the Bergamasc Alps (Calcare Rosso, Italy). Italian Journal of Geoscience 133, 294-314.

Warren J., 2000. Dolomite: Occurrence, evolution and economically important associations, Earth-Science Reviews 52, 1-81.

Webb, G.E., Kamber, B.S., 2000. Rare earth elements in Holocene reefal microbialites: a new shallow seawater proxy. Geochimica et Cosmochimica Acta 64, 1557-1565.

Webb, G.E., Nothdurft, L.D., Kamber, B.S., Kloprogge, J.T., Zhao, J.-X. 2009. Rare earth element geochemistry of scleractinian coral skeleton during meteoric diagenesis: a before

and after sequence through neomorphism of aragonite to calcite. Sedimentology 56, 1433-1463

Wilson, T. R. S., 1975. Salinity and the major elements of sea water. In Chemical oceanography, 2nd ed., vol. 1, ed., J. P. Riley and G. Skirrow, London, Academic Press, pp. 365-413.

Zhong, S., Mucci, A., 1995. Partitioning of rare earth elements (REEs) between calcite and seawater solutions at 25 C and 1 atm, and high dissolved REE concentrations. Geochimica et Cosmochimica Acta. 59(3), 443-453.

List of figures and tables

Fig. 1. Late Ladinian (below, modified after Berra et al., 2011) and early Carnian (above, modified after Brusca et al., 1981) palaeogeography of the western Southern Alps with inset of simpliýed tectonic map of Northern Italy (modiýed from Ronchi et al., 2011).

Fig. 2. Facies and stratigraphic framework of Middle-Upper Triassic sediments of the western Southern Alps (modified from Assereto and Folk, 1980).

Fig. 3. Photomicrographs of petrographic features of Esino and Breno carbonates. (a) Calcite C1 (plane polarized; Sample PE1), (b) Calcite C2 and fibrous cement F (crossed polars; Sample PE7), (c) Cathodoluminescence image of (b) showing dull CL of C1 and C2, (d) Dolomite D1 and D2 (crossed polars; Sample ES), (e) Dolomite D1, D3a and calcite C3 (plane polarized; Sample PE8), (f) Cathodoluminescence image of (e) showing dull CL in D1 and D3a, (g) Dolomite D2a, D2b and calcite C3 showing organic matter along zones in D2a crystals (plane polarized; Sample BR), (h) Cathodoluminescence image of (g) showing dull CL of D2a, zonation CL of D2 and bright orange CL of C3, (i) Saddle dolomite D3b with

undulose extinction (crossed polars; Sample BR3), (j) Cathodoluminescence image of (i) showing zonation CL of D3b, (k) D2 with organic material around the crystal rim (crossed polars; Sample BR), and (l) Ultraviolet image of (k) showing no þorescence of the organic matter.

Fig. 4. Paragenetic sequence of the main diagenetic events that influenced the Esino and Breno carbonates based on petrographic relationships.

Fig. 5. Plots of the microthermometric data of primary two-phase þuid inclusions trapped in D2, D3 and C3, showing histograms of homogenization temperature of (a) D2, (b) D3, and (c) C3, and a scatter diagram (d) of estimated salinity (Bodnar, 2003) vs. homogenization temperatures of D2 and D3.

Fig. 6. Pattern of mean shale-normalized REE concentrations of the investigated calcite and dolomite generations.

Fig. 7. Scatter diagram of ŭ^{18}O vs. ŭ^{13}C of the investigated carbonates. The square marks the ŭ^{18}O and ŭ^{13}C ranges of composition of the well-preserved Triassic carbonates (Korte et al., 2005)

Fig. 8. Scatter diagrams of ŭ^{13}C vs. Mn/Sr of all of the investigated dolomites.

Fig. 9. Temperature (*T*) vs. ŭ^{18}O $_{\text{dagenetic þuid}}$. ŭ^{18}O $_{\text{dolomite}}$ values reconstructed following the equation of Land, 1983 ($10^3 \ln Ŭ = 3.2\times10^6 T^{-2}$-3.3). The shaded areas indicate the ranges of ŭ^{18}O$_{\text{þuid}}$ based on the ŭ^{18}O$_{\text{dolomite}}$ values and homogenization temperatures (T_h) of each dolomite generation.

Fig. 10. Scatter diagram of $(Ce/Ce^*)_{SN}$ vs $(Pr/Pr^*)_{SN}$ for the precursor lime mudstone (C1) and all of the investigated dolomites (after Bau and Dulski, 1996). Detail in text.

Fig. 11. Scatter diagrams of (a) N_2/Ar vs. CO_2/CH_4 and (b) N_2/Ar vs. Ar/He for C1 and dolomites (D1, D2, and D3) of the Esino and Breno formations (after Norman and Moore, 1999; Blamey and Norman, 2002; Blamey, 2012) based on the weighted mean values (Appendix 3).

Table 1. Statistics of microthermometric measurements of the investigated carbonates.

Table 2. $CaCO_3$, $MgCO_3$, Mn, Sr, Fe, ŭ^{18}O and ŭ^{13}C statistics of the investigated Esino and Breno carbonates in the western Southern Alps.

Table 3. Summary of rare earth element concentrations in the Esino and Breno carbonates in the western Southern Alps

Table 4. Summary of statistics of Ce $(Ce/Ce^*)_{SN}$, Eu $(Eu/Eu^*)_{SN}$ and La $(Pr/Pr^*)_{SN}$ anomalies based on the equations of Bau and Dulski (1996).

Table 5. Summary of quantitative þuid-inclusion gas analyses (in mol %) using a burst-size weighted mean of several replicate analyses from the investigated samples. Detail in text.

Table 6. Results of the halogen contents and F/Cl and Cl/Br molar ratios of the investigated Esino and Breno carbonates.

Appendix 1. Sample, elemental, isotopic geochemical and REE compositions of Esino and Breno carbonates.

Appendix 2. Results of fluid-inclusion microthermometric measurements of Esino and Breno carbonates.

Appendix 3. Fluid-inclusion gas data of Esino and Breno carbonates.